AGU PUBLICATIONS

Journal of Advances in Modeling Earth Systems

RESEARCH ARTICLE

10.1002/2016MS000842

This article is a companion to *Nusbaumer et al.* [2017], doi:10.1002/2016MS000839.

Key Points:
- Water isotope physics have been added to the version 4 of the Community Land Model
- An imperfect soil moisture simulation has limited impacts on soil water isotopic profiles
- Soil evaporative kinetic effect alone cannot rectify coupled model discrepancy with respect to water isotopic data

Supporting Information:
- Supporting Information S1
- Data Set S1
- Data Set S2

Correspondence to:
T. E. Wong,
twong@psu.edu

Citation:
Wong, T. E., J. Nusbaumer, and D. C. Noone (2017), Evaluation of modeled land-atmosphere exchanges with a comprehensive water isotope fractionation scheme in version 4 of the Community Land Model, *J. Adv. Model. Earth Syst.*, *9*, 978–1001, doi:10.1002/2016MS000842.

Received 22 OCT 2016
Accepted 22 MAR 2017
Accepted article online 31 MAR 2017
Published online 28 APR 2017

Evaluation of modeled land-atmosphere exchanges with a comprehensive water isotope fractionation scheme in version 4 of the Community Land Model

Tony E. Wong[1,2,3], Jesse Nusbaumer[2,4,5], and David C. Noone[2,4,6]

[1]Department of Applied Mathematics, University of Colorado, Boulder, Colorado, USA, [2]Cooperative Institute for Research in Environmental Sciences, University of Colorado, Boulder, Colorado, USA, [3]Now at: Earth and Environmental Systems Institute, Pennsylvania State University, University Park, Pennsylvania, USA, [4]Department of Atmospheric and Oceanic Sciences, University of Colorado, Boulder, Colorado, USA, [5]Now at: NASA Goddard Institute for Space Studies, New York, New York, USA, [6]Now at: College of Earth, Ocean, and Atmospheric Sciences, Oregon State University, Corvallis, Oregon, USA

Abstract All physical process models and field observations are inherently imperfect, so there is a need to both (1) obtain measurements capable of constraining quantities of interest and (2) develop frameworks for assessment in which the desired processes and their uncertainties may be characterized. Incorporation of stable water isotopes into land surface schemes offers a complimentary approach to constrain hydrological processes such as evapotranspiration, and yields acute insight into the hydrological and biogeochemical behaviors of the domain. Here a stable water isotopic scheme in the National Center for Atmospheric Research's version 4 of the Community Land Model (CLM4) is presented. An overview of the isotopic methods is given. Isotopic model results are compared to available data sets on site-level and global scales for validation. Comparisons of site-level soil moisture and isotope ratios reveal that surface water does not percolate as deeply into the soil as observed in field measurements. The broad success of the new model provides confidence in its use for a range of climate and hydrological studies, while the sensitivity of simulation results to kinetic processes stands as a reminder that new theoretical development and refinement of kinetic effect parameterizations is needed to achieve further improvements.

1. Introduction

Recent years have seen the proliferation of field deployable instruments capable of making measurements of stable water isotope ratios. The computational power necessary to run elaborate model simulations of ecosystems more representative of natural systems from which measurements originate has also become more widely available. These advances heighten the importance of developing tools at their interface, specifically for the synthesis of measurements of stable water isotopic ratios and isotopically enabled model simulations. The availability of water isotopic measurements at high-temporal resolution provides a means to validate the land surface schemes [*Griffis*, 2013]. These isotope-enabled land surface models provide an opportunity to gain unique insight into hydrological processes and biogeochemical behaviors of ecosystems. For example, land-based water isotopic data are commonly used to partition evapotranspiration (ET) flux into evaporation and transpiration components [*Ferretti et al.*, 2003; *Yepez et al.*, 2003; *Williams et al.*, 2004; *Wang et al.*, 2010; *Jasechko et al.*, 2013; *Sutanto et al.*, 2014; *Wei et al.*, 2015; *Good et al.*, 2015]. Water isotopic data may also be leveraged in isotopically enabled climate models to diagnose key model shortcomings [*Risi et al.*, 2012]. Furthermore, it has been shown that through improved simulation of the below-canopy isotopic exchanges between surface and canopy air-space, better agreement between modeled and observed isotope ratios may be achieved [*Aemisegger et al.*, 2015; *Sutanto et al.*, 2014].

We present a tracer hydrological scheme incorporated into the National Center for Atmospheric Research's (NCAR) version 4 of the Community Land Model (CLM4) [*Oleson et al.*, 2010]. This model, iCLM4, closely parallels the native hydrology in CLM4, with several essential additions which enable the modeling of hydrological tracers. Here "iCLM4" denotes the isotopic model version, while "CLM4" is reserved for the underlying nonisotopic model. These tracers may be temporal (such as tracing summer rainfall through the

hydrological cycle), spatial (such as tracing rain reevaporation from the Amazon rainforest), or isotopic (tracing water isotopologues). The focus of the present work is on the latter, specifically heavy water isotopes HDO and $H_2^{18}O$. This parallel tracer hydrology approach was also followed by *Haese et al*. [2013] in the implementation of their isotopically enabled ECHAM5-JSBACH model. These authors noted the need to resolve the vertical structure within the soil water isotopic simulation, as well as the need for observations of soil moisture and its isotopic composition to validate such a scheme. The isotope-enabled ORCHIDEE land surface model of *Risi et al*. [2016] found a similar sensitivity of their modeled soil water isotope ratios to the infiltration pathways and evaporative fraction of soil water. *Risi et al*. [2016] suggest that water isotopic measurements be leveraged to constrain such hydrological processes in land surface models. The isotope-enabled NASA-GISS ModelE Land Surface Model found a need for multilayer observations of isotope ratios in soil moisture, as well as global data sets to validate the coupled model as a whole [*Aleinov and Schmidt*, 2006]. The iCLM4 model and experiments described here make progress toward fulfilling these needs, and examinations of uncertainties in the global as well as local soil isotopic simulation will be presented.

This work is organized as follows: Section 2.1 provides a technical review of the isotope tracer model implemented in iCLM4, with some review of key parameterizations from CLM4. Section 3.1.1 outlines the site-level data used for validation of the model results, and section 3.1.2 provides a detailed process-level comparison between these data and model results. Section 3.2.1 gives a description of a set of global-scale model experiments to assess model performance and sensitivity by coupling the isotopic land surface scheme reviewed in the present work with the complementary stable water isotope-enabled atmospheric model [*Nusbaumer et al*., 2017]. The data sets used for this comparison are reviewed in section 3.2.2, and results are presented in section 3.2.3. Model simulations are compared using data sets that span the global domain as well as a more complete and high frequency set for a specific site. It will be shown that the iCLM4 model illuminates strengths and shortcomings in the parameterizations of evaporation and soil hydrology in CLM4, and these key findings were attainable through incorporation of the water tracer scheme implemented here. A review of the practical implications of these results and future work is given in section 4.

2. Methods

2.1. Isotope Model for Terrestrial Water Exchange

In CLM4, each model gridcell is composed of landunits, which include glacier, lake, wetland, urban, and vegetated [*Oleson et al*., 2010]. Note that vegetated landunits include bare soil. In the isotope scheme described here, the glacier, lake, wetland, and urban landunits treat all water species tracers identically, and do not fractionate. This simplifying assumption is made as a step toward parameterizing the first-order effects of the land surface, the vegetated land areas. Glaciers, lakes, wetlands, and urban land areas are, of course, also fractionating, but the attention of the present study, in particular the comparison of model output to observational data, is restricted to vegetated areas.

Figure 1 depicts the main iCLM4 isotopic water pools (light blue) and fluxes between them (arrows). Each water flux in the model is accompanied by an analogous water isotopic flux. The interested reader is directed to *Oleson et al*. [2010] for more detailed discussion and schematics (specifically their Figure 1.2) of the CLM4 hydrology. Only the parts most relevant to the water isotopic scheme are mentioned in the following model description. The essence of the isotopic tracer scheme is to estimate these water isotopic fluxes between the atmosphere and land surface (evaporation from soil, evaporation of water intercepted by the canopy, and transpiration), and consequently predict the isotopic composition of all water pools. At the end of each model time step, the mass of all isotope species is checked to ensure the change in storage in soil, snow, and canopy-intercepted water is equal to the input from rain and snow, minus the output to evapotranspiration and surface and subsurface runoff.

Let i refer to any specific water isotopologue, $H_2^{16}O$, HDO, or $H_2^{18}O$. Surface evaporation, E_g^i, transports water between the surface soil (or top snow pack layer) and the canopy air-space. Transpiration through sunlit and shaded leaves, $E_{v,sun}^i$ and $E_{v,sha}^i$, respectively, transports water from within leaves to the canopy air-space. Evaporation of canopy-intercepted water, E_c^i, moves water between the surface of leaves to the canopy air-space. E^i denotes the transfer of moisture between the canopy air-space and the above-canopy

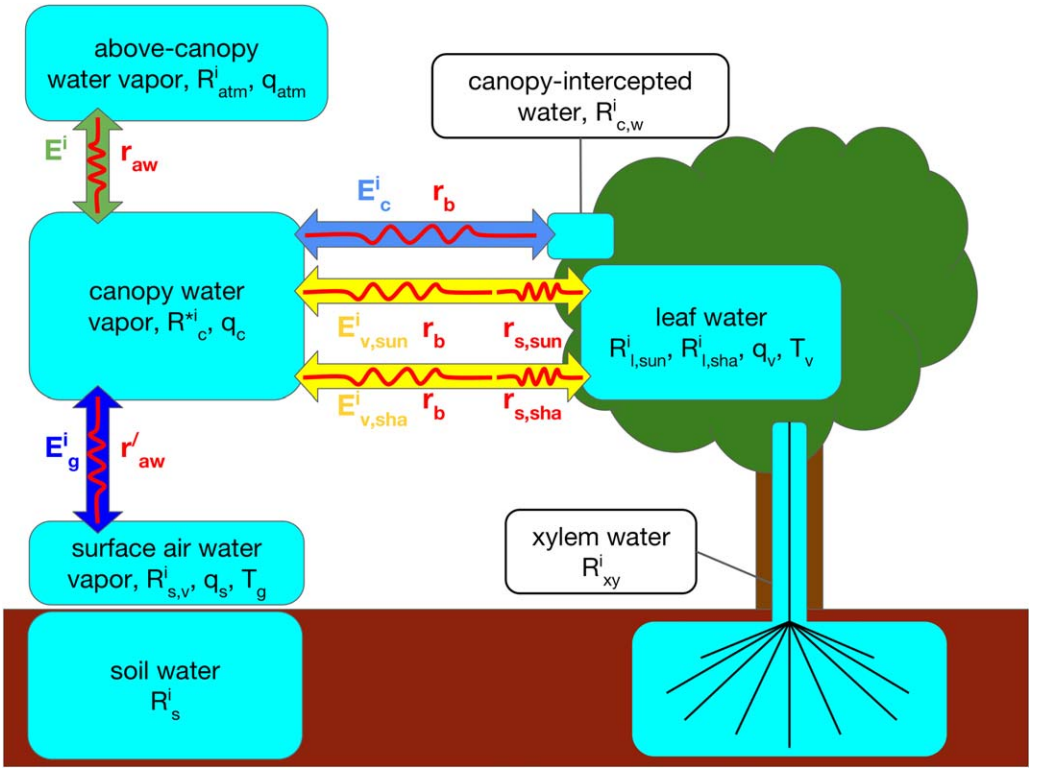

Figure 1. Schematic of ecosystem water pools (blue boxes), resistances to moisture and heat transport (red resistors), moisture fluxes (thick arrows), isotope ratios (R), humidities (q), and temperatures (T).

air-space. When coupled to an isotopically enabled atmospheric circulation model, E^i is provided to the atmospheric model; precipitation and near-surface isotopic mixing ratio are provided to iCLM4 as inputs. For $i = {}^{16}O$, the water isotopic fluxes (and other quantities calculated below) reduce to those for bulk water. The balance of these five fluxes in the canopy air-space is illustrated in Figure 1 and may be expressed as

$$E^i = E^i_g + E^i_{v,sun} + E^i_{v,sha} + E^i_c. \tag{1}$$

CLM4 stores water on the landscape in three distinct reservoirs: soil water, snowpack, and water intercepted by the canopy. Conservation of mass (equation (2)) and Darcy's Law (equation (3)) govern the soil moisture parameterization, for both bulk water and isotopic water, and are combined to yield a Richards equation for the soil water isotopic fluxes throughout the soil column, modified by a moisture sink term (equation (4)). In equations (2)–(4), $\theta(z,t)$ is the soil water content of the soil at depth z and time t ($mm^3\ mm^{-3}$); $q(z,t)$ is the water flux from the current soil layer to the one below it ($mm\ s^{-1}$); $Q(z,t)$ is a soil moisture sink term (e.g., evaporation) ($mm\ s^{-1}$); $k(z,t)$ is hydraulic conductivity ($mm\ s^{-1}$); $\psi(z,t)$ is the soil matric potential (mm); and $\psi_E(z,t)$ is the equilibrium state soil matric potential (mm). Further details regarding the bulk water hydrological parameterizations in CLM4 may be found in *Oleson et al.* [2010]

$$\frac{\partial\theta(z,t)}{\partial t} = -\frac{\partial q(z,t)}{\partial z} - Q(z,t), \tag{2}$$

$$q(z,t) = -k(z,t)\left[\frac{\partial(\psi(z,t)+z)}{\partial z}\right], \tag{3}$$

$$\frac{\partial\theta(z,t)}{\partial t} = \frac{\partial}{\partial z}\left[k(z,t)\left(\frac{\partial(\psi(z,t)-\psi_E(z,t))}{\partial z}\right)\right] - Q(z,t), \tag{4}$$

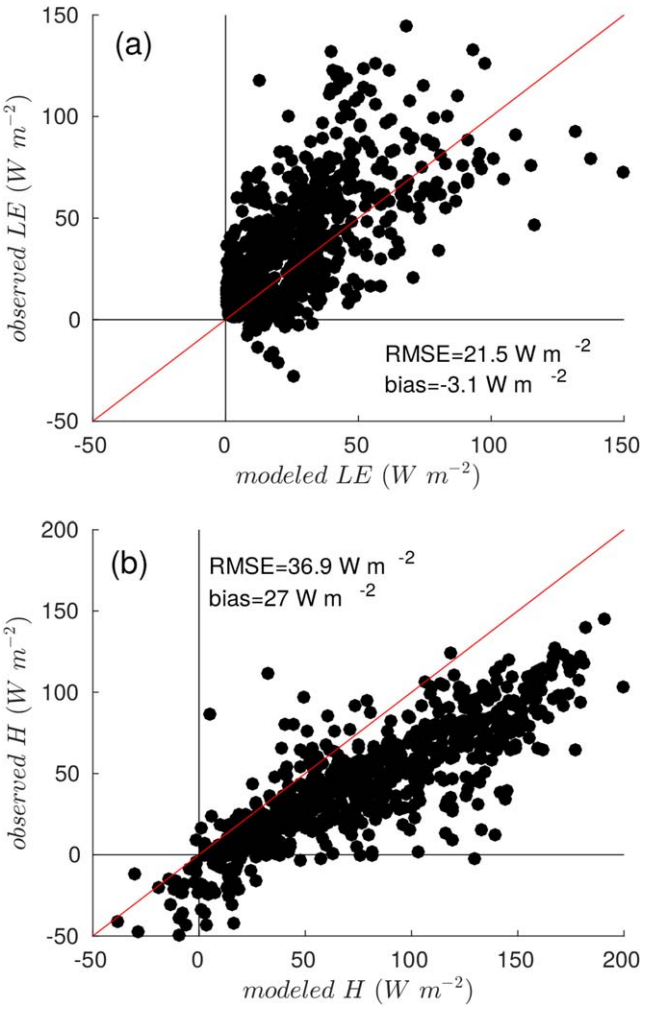

Figure 2. Comparison between modeled and observed (a) latent heat flux (LE) and (b) sensible heat flux (H) for BAO. The line indicates a one-to-one relationship.

The continuous equations are discretized on 20 model levels and solved numerically [*Oleson et al.*, 2010]. The fluxes between soil layers are linearized about the moisture content of those layers to create a tridiagonal system of equations in terms of the soil moisture. This system is solved using the Crank-Nicolson method [*Crank and Nicolson*, 1947].

After the bulk soil moisture update (above), each layer's soil water isotope ratios are then updated. This is done by dividing the model time step into n_{sub} substeps to maintain numerical stability. The default soil time substep is one second. This step size was determined to ensure the result for the isotopic substep calculation for $H_2^{16}O$ in iCLM4 came into agreement with the bulk water calculation by CLM4. The total moisture fluxes between all adjacent soil layers are known, from conservation of mass and the surface boundary condition (soil infiltration and evaporation are known). During each time substep, $1/n_{sub}$ of the total moisture fluxes are moved between adjacent soil layers, and interfacial fluxes carry the isotopic ratios from their layers of origin. After each substep, the isotope ratios of each soil layer are updated.

2.1.1. Isotopic Kinetic Fractionation Factor

Two main parameterizations are used for the isotopic kinetic fractionation factor, α_k^i. The first is:

$$\alpha_k^i = \left(\frac{D^i}{D}\right)^n, \; n \text{ constant} \tag{M78}$$

In (M78), i refers to the isotopic species, D and D^i are the molecular diffusivities of the light and heavy isotopologue, respectively [*Merlivat*, 1978], and the exponent n is chosen between 0 and 1 to reflect the balance of turbulent versus molecular diffusive transport for the water movement between the two isotopic reservoirs in question. *Williams et al.* [2004] use $n = 1$ for evaporation from dry soils, where diffusion through the dry soil matrix is the primary form of moisture transfer, and $n = 1/2$ for evaporation from wet soil. In purely turbulent conditions, $n = 0$ is appropriate, because turbulent mixing treats all isotopic species equally, regardless of differing molecular properties [*Noone and Sturm*, 2010]. Although the optimal choice for the exponent n for a given set of environmental conditions is an area of ongoing study, (M78) remains a popular choice [*Roden et al.*, 2000; *Wang and Yakir*, 2000; *Williams et al.*, 2004; *Xu et al.*, 2008; *Buenning et al.*, 2014; *Rothfuss et al.*, 2010].

The second formulation is adapted from the parameterization of kinetic fractionation for evaporation from rough ocean surfaces given by *Merlivat and Jouzel* [1979] (cf., their Figure 2):

$$k^{18_O} = \begin{cases} 8.82u_* + 0.472, & \text{if } R_e \geq 1 \\ 6, & \text{if } R_e < 1 \end{cases},$$
$$k^D = 0.88k^{18_O},$$
$$k^{16_O} = 0,$$
$$\alpha_k^i = \frac{1000 - k^i}{1000}. \quad \text{(MJ79)}$$

In (MJ79), R_e is the Reynolds number, which represents whether the land surface conditions are smooth ($R_e < 1$) or rough ($R_e \geq 1$), and u_* is the friction velocity (m s^{-1}). This model differs from (M78) by capturing the partitioning of diffusive versus turbulent transport as a function of the Reynolds number rather than treating it as a constant. The equation given above for k^{18_O} (‰) is a linear fit for the results presented in Figure 2 of *Merlivat and Jouzel* [1979]. A similar approach was followed by *Haese et al*. [2013]. In iCLM4, (MJ79) is used, and the benefits and sensitivities of this choice are assessed below.

2.1.2. Isotopic Composition of Evaporation and Transpiration

2.1.2.1. Bare Ground Fluxes

This section describes the formulation of the water isotopic evaporative flux over bare soil. Let E_g refer to the evaporation flux of $H_2^{16}O$, as calculated by native CLM4. The isotopic evaporation flux (kg m^{-2} s^{-1} is based on the model of *Craig and Gordon* [1965]:

$$E_g^i = c_g^i \left[\left(f_{s,eq} \frac{R_s^i q_g}{\alpha^i(T_g)} + (1 - f_{s,eq}) R_{atm}^i q_{atm} \right) - R_{atm}^i q_{atm} \right]. \quad (5)$$

q_g is the specific humidity of the air at the ground surface; q_{atm} is the atmospheric specific humidity; c_g^i is the water isotopic conductance between the evaporating surface and the above-canopy air-space; α^i is the equilibrium fractionation factor at T_g, the temperature of the evaporating surface [*Horita and Wesolowski*, 1994]; R_{atm}^i is the isotope ratio of the atmospheric water vapor; and R_s^i is the isotope ratio of the total soil water and ice on the evaporating surface. The case where $q_{atm} > q_g$ represents dew or frost formation. Ice is included in the calculation to account for possible sublimation or dew/frost onto snow or ice. Neither kinetic nor equilibrium fractionation is applied to sublimation. $f_{s,eq}$ ranges from 0 to 1 and is the fraction of tracer evaporation source water which is not in equilibrium with the tracer atmospheric water vapor, which accounts for partial isotopic equilibration between evaporation source and destination water. $f_{s,eq}$ is taken to be one for evaporation from bare soils (implying no partial equilibration and reduction to the original model of *Craig and Gordon* [1965]). For evaporation from vegetated soils, $f_{s,eq}$ is calculated as an exponential decay, with rate constant given by the ratio of the atmospheric water vapor content to the moisture content of the surface soil layer. When $f_{s,eq} = 0$, the evaporative flux is zero, and isotopic exchange brings soil water into equilibrium with canopy water at a rate given by the canopy conductance. This avoids the problem that the *Craig and Gordon* [1965] formulation for the evaporation assumes that the liquid reservoir is infinite, which is not valid in all cases. That is, both the soil water content and the isotopic composition can change dramatically over a single time step, which needs to be taken into account to both ensure numerical stability and correctly model the physical system.

The Monin-Obukhov stability iteration used in CLM4 results in an aerodynamic resistance to moisture and heat transport from surface to above-canopy air-space, r_{aw} (s m^{-1}). The water isotopic conductance is then

$$c_g^i = \begin{cases} \alpha_k^i \frac{1}{r_{aw}}, & \text{if } q_{atm} > q_g \\ \alpha_k^i \frac{\beta_{soi}}{r_{aw}}, & \text{if } q_{atm} \leq q_g \end{cases}, \quad (6)$$

where β_{soi} ranges from 0 to 1 and represents the limitation on evaporation below the potential evaporation rate when soil is nonsaturated [*Oleson et al*., 2010; *Sakaguchi and Zeng*, 2009], and α_k^i is the isotopic kinetic fractionation factor for isotopic species *i*. For bare ground evaporation, α_k^i is parameterized following (MJ79).

2.1.2.2. Vegetated Fluxes

A cornerstone of the fractionation scheme in iCLM4 is the formulation of the total water isotopic fluxes between the land and the atmosphere as the sum of surface evaporation, vegetation transpiration, and evaporation of canopy-intercepted water for vegetated surfaces, as in equation (1). For each isotopic species, *i*, a five-way water isotopic mass balance in the vegetation canopy is solved between: (1) ground

evaporation (E^i_g), (2) evaporation of canopy-intercepted water (E^i_c), (3 and 4) sunlit and shaded leaf transpiration ($E^i_{v,sun}$ and $E^i_{v,sha}$), and (5) coupling flux to the atmosphere (E^i). This calculation originates from *Riley et al.* [2002], although iCLM4 supports the additional flux of evaporation of canopy-intercepted water, and an analytic solution has been found to simultaneously compute leaf water and canopy air-space isotopic ratios. These fluxes are based on the model of *Craig and Gordon* [1965], and modified to include partial isotopic equilibration and the mass balance of *Flanagan et al.* [1991]. For a given isotopic species, *i*, the total water isotopic ecosystem flux, E^i (equation (1)), and its constituents are

$$E^i = \rho_{atm} c^i_a \left(R^{*i}_c q_c - R^i_{atm} q_{atm} \right), \tag{7}$$

$$E^i_g = \rho_{atm} c^i_g \left(c_{al,0} \left(f_{s,eq} R^i_{s,v} + (1 - f_{s,eq}) R^{*i}_c \right) q_g - c_{l,0} R^{*i}_{leaf} q_{sat,l}(T_v) - c_{a,0} R^i_{atm} q_{atm} \right), \tag{8}$$

$$E^i_c = \rho_{atm} c^i_c \left[\left(f_{c,eq} \frac{R^i_{c,w}}{\alpha^i(T_v)} + (1 - f_{c,eq}) R^{*i}_c \right) q_{sat,l}(T_v) - R^{*i}_c q_c \right], \tag{9}$$

$$E^i_{v,sun} = \rho_{atm} c^i_{sun} \left(\frac{R^{*i}_{l,sun} q_{sat,l}(T_v)}{\alpha^i(T_v)} - R^{*i}_c q_c \right), \tag{10}$$

$$E^i_{v,sha} = \rho_{atm} c^i_{sha} \left(\frac{R^{*i}_{l,sha} q_{sat,l}(T_v)}{\alpha^i(T_v)} - R^{*i}_c q_c \right), \tag{11}$$

In equations (7)–(11), R^{*i}_c is the isotope ratio of the canopy water vapor when the transpirative outflow from vegetation is in isotopic steady state with the root uptake inflow; $R^{*i}_{l,sha}$ and $R^{*i}_{l,sun}$ are the as yet unknown isotope ratios of the sunlit and shaded leaf water, respectively, at steady state. R^{*i}_{leaf} is the leaf area index (LAI)-weighted average (sunlit/shaded) leaf water isotope ratio at steady state; R^i_{atm} is the isotope ratio of the atmospheric water vapor (above-canopy water vapor); $R^i_{s,v}$ is the isotope ratio of the evaporation front water vapor (currently taken to be surface soil); $R^i_{c,w}$ is the isotope ratio of the canopy-intercepted water (i.e., water pooling on a leaf); $\alpha^i(T_v)$ is the equilibrium fractionation factor at the temperature of the vegetation (T_v) [*Horita and Wesolowski*, 1994]; $f_{c,eq}$ ranges from 0 to 1 and is the fraction of tracer canopy-intercepted water which is not in isotopic equilibrium with the tracer canopy water vapor; q_{atm} is the atmospheric specific humidity; $q_{sat,l}(T_v)$ is the saturated specific humidity at the temperature of the transpiring vegetation; q_g is the specific humidity at the evaporation front; q_c is the specific humidity in the canopy air-space; ρ_{atm} is the atmospheric mass density; c^i_a is the water isotopic conductance between the canopy and above-canopy air-spaces; c^i_g is the water isotopic conductance between the evaporating surface and canopy air-spaces; c^i_c is the water isotopic conductance between the canopy-intercepted water and canopy air-spaces; c^i_{sun} and c^i_{sha} are the water isotopic conductances between the sunlit and shaded leaf interiors and the canopy air-space, respectively; $c_{al,0}$ is the sum of the normalized conductances for the light isotopologue through the canopy to above-canopy air-spaces ($c_{a,0}$) and through the leaf air-space ($c_{l,0}$). The parameterization for the steady state isotope ratios of sunlit and shaded leaf water is from *Flanagan et al.* [1991]:

$$R^{*i}_{l,sun} = \alpha^i(T_v) \left(\frac{q_{sat,l}(T_v) - q_{l,sun}}{q_{sat,l}(T_v)} \frac{R^i_{xy}}{\alpha^i_{k,s}} + \frac{q_{l,sun} - q_c}{q_{sat,l}(T_v)} \frac{R^i_{xy}}{\alpha^i_{k,b}} + \frac{q_c}{q_{sat,l}(T_v)} R^{*i}_c \right), \tag{12}$$

$$R^{*i}_{l,sha} = \alpha^i(T_v) \left(\frac{q_{sat,l}(T_v) - q_{l,sha}}{q_{sat,l}(T_v)} \frac{R^i_{xy}}{\alpha^i_{k,s}} + \frac{q_{l,sha} - q_c}{q_{sat,l}(T_v)} \frac{R^i_{xy}}{\alpha^i_{k,b}} + \frac{q_c}{q_{sat,l}(T_v)} R^{*i}_c \right), \tag{13}$$

where $q_{l,sun}$ and $q_{l,sha}$ are the specific humidities within the sunlit and shaded leaves, respectively; and $\alpha^i_{k,s}$ and $\alpha^i_{k,b}$ are the kinetic fractionation factors for moisture diffusion through vegetation stomata ((M78), $n = 1$) and through the laminar leaf boundary layer ((M78), $n = 2/3$), respectively [*Roden et al.*, 2000; *Flanagan et al.*, 1991]. R^i_{xy} is the isotope ratio of vegetation xylem water, which is calculated as the soil column-averaged soil water isotope ratio, weighted by the vegetation rooting depth profile at each soil layer. Equations (12) and (13) can be substituted into equations (7)–(11), which can in turn be substituted into equation (1) to obtain the unknown R^{*i}_c to provide a solution that assumes isotopic steady state. This steady state assumption, while often valid near midday in highly productive ecosystems, can be relaxed, and the nonsteady solution is given below. It remains, however, to select the conductances that capture the isotopic kinetic effects.

2.1.2.3. Conductances and Kinetic Effects

The water isotopic conductances follow the native CLM4 calculation for their bulk water analogs:

$$c_a^i = \frac{f_{veg}}{\left(\frac{r_{aw}}{\alpha_{k,a}^i}\right)}, \tag{14}$$

$$c_l^i = \frac{f_{veg}(L+S)}{\frac{r_b}{\alpha_{k,b}^i}} r'', \tag{15}$$

$$c_g^i = \begin{cases} \dfrac{f_{veg}}{\frac{r'_{aw}}{\alpha_{k,g}^i} + \frac{r_{litter}}{\alpha_{k,litter}^i}}, & \text{if } q_{atm} > q_g \\ \dfrac{\beta_{soi} f_{veg}}{\frac{r'_{aw}}{\alpha_{k,g}^i} + \frac{r_{litter}}{\alpha_{k,litter}^i}}, & \text{if } q_{atm} \le q_g \end{cases}, \tag{16}$$

where f_{veg} is the fraction of the land surface which is vegetated but not covered in snow; L and S are the leaf and stem area indices, respectively; r_{aw} is the aerodynamic resistance between the canopy air-space and above-canopy (GCM) air-space; r'_{aw} is the aerodynamic resistance between the surface air-space and canopy air-space; r_{litter} is a leaf litter resistance; r_b is the leaf boundary layer resistance; and r'' is the fraction of potential evaporation from transpiration. Further information regarding the parameterization of all nonisotope-specific terms may be found in *Oleson et al.* [2010]. $\alpha_{k,litter}^i$ is by default equal to 1, representing a null hypothesis of no fractionation as moisture evaporates through the dry litter layer. $\alpha_{k,a}^i$ follows (M78) with $n = 0$ because exchange between canopy and above-canopy air-spaces is dominated by turbulence [*Lee et al.*, 2009]. $\alpha_{k,g}^i$ is parameterized by (MJ79). In order to be consistent with the original formulation of *Merlivat and Jouzel* [1979], the kinetic factor of (MJ79) is rescaled to act over the entire surface to above-canopy air-space, instead of only surface to canopy.

Given the bulk vegetation transpiration (E_v) and evaporation of canopy-intercepted water (E_c) fluxes of $H_2^{16}O$ calculated, effective conductances for these fluxes may be calculated in a manner consistent with the bulk fluxes (equations (17) and (18)). Using f_{sun}, the fraction of leaves which are sunlit, the bulk transpiration flux is then divided into sunlit and shaded leaf components (equations (19) and (20)):

$$c_c = \frac{E_c}{\rho_{atm}(q_{sat,l} - q_c)}, \tag{17}$$

$$c_t = \frac{E_v}{\rho_{atm}(q_{sat,l} - q_c)}, \tag{18}$$

$$c_{sun} = f_{sun} c_t, \tag{19}$$

$$c_{sha} = (1 - f_{sun}) c_t, \tag{20}$$

Now the effective conductances for isotopic species i are related to the bulk conductances as follows:

$$c_{sun}^i = \frac{c_{sun}}{r''} f_{dry} r_b \left(\frac{\left(\frac{L_{sun}}{L_{sun}+L_{sha}}\right)}{\frac{r_b}{\alpha_{k,b}^i} + \frac{r_{s,sun}}{\alpha_{k,s}^i}} + \frac{\left(\frac{L_{sha}}{L_{sun}+L_{sha}}\right)}{\frac{r_b}{\alpha_{k,b}^i} + \frac{r_{s,sha}}{\alpha_{k,s}^i}} \right), \tag{21}$$

$$c_{sha}^i = \frac{c_{sha}}{r''} f_{dry} r_b \left(\frac{\left(\frac{L_{sun}}{L_{sun}+L_{sha}}\right)}{\frac{r_b}{\alpha_{k,b}^i} + \frac{r_{s,sun}}{\alpha_{k,s}^i}} + \frac{\left(\frac{L_{sha}}{L_{sun}+L_{sha}}\right)}{\frac{r_b}{\alpha_{k,b}^i} + \frac{r_{s,sha}}{\alpha_{k,s}^i}} \right), \tag{22}$$

$$c_c^i = \alpha_{k,c}^i c_c, \tag{23}$$

f_{dry} is the fraction of foliage that is green and dry, and $\alpha_{k,c}^i$ is given by (M78) with $n = 2/3$. r'' is the fraction of potential evaporation from transpiration for $H_2^{16}O$, and given by

$$r'' = f_{dry} r_b \left(\frac{\left(\frac{L_{sun}}{L_{sun}+L_{sha}}\right)}{r_b + r_{s,sun}} + \frac{\left(\frac{L_{sha}}{L_{sun}+L_{sha}}\right)}{r_b + r_{s,sha}} \right). \tag{24}$$

Substituting equations (7)–(13) into equation (1) permits solving for R_c^{*i}, the isotope ratio of the canopy water vapor at steady state. Algebra reveals

$$\begin{aligned} R_c^{*i} = [& c_{sun}^i \left((q_{sat,l} - q_{l,sun}) \frac{1}{\alpha_{k,s}^i} + (q_{l,sun} - q_c) \frac{1}{\alpha_{k,b}^i}) \right) R_{xy}^i \\ & + c_{sha}^i \left((q_{sat,l} - q_{l,sha}) \frac{1}{\alpha_{k,s}^i} + (q_{l,sha} - q_c) \frac{1}{\alpha_{k,b}^i}) \right) R_{xy}^i \\ & + c_g^i f_{s,eq} R_{s,v}^i q_g + c_c^i \frac{f_{c,eq} R_{c,w}^i q_{sat,l}(T_v)}{\alpha^i(T_v)} + c_a^i R_{atm}^i q_{atm}] / \\ & [(1 - c_{sun}^i - c_{sha}^i) q_c - c_g^i (1 - f_{s,eq}) q_g - c_c^i (1 - f_{c,eq}) q_{sat,l}(T_v)] . \end{aligned} \tag{25}$$

Equations (12) and (13) are used to determine the steady state leaf water isotope ratios ($R_{l,sun}^{*i}$ and $R_{l,sha}^{*i}$). The isotope ratios of the canopy-intercepted liquid water ($R_{c,w}^i$) and soil water vapor ($R_{s,v}^i$) are determined using R_c^{*i} and $f_{s,eq}$ and $f_{c,eq}$. Finally, equations (7)–(11) are used to determine the water isotopic fluxes.

The isotope ratios of the leaf water, canopy-intercepted water, surface water vapor, and canopy water vapor are all in isotopic steady state. The Peclet effect describes the opposing tendencies within leaves between evaporatively enriched water at evaporation sites within leaves and inflowing unenriched xylem water [*Farquhar and Lloyd*, 1993]. It has been shown that including the Peclet effect in the calculation of isotope ratios in leaf water leads to better agreement with observations of leaf water isotope ratios [*Farquhar and Lloyd*, 1993; *Cernusak et al*., 2005]. The latter authors also found that their steady state model with Peclet effect approximated the nonsteady state reasonably well. To this end, the steady state leaf water isotope ratios are inputs to a diagnostic calculation of these nonsteady state ratios, accounting for the Peclet effect. In iCLM4, it is left as an option whether to use these Peclet-included leaf water isotope ratios in the prognostic physics calculations or leave as a purely diagnostic quantity.

It has been consistently noted that the assumption of isotopic steady state is not always realized in the field [*Buenning et al*., 2014; *Cernusak et al*., 2005; *Wang and Yakir*, 2000]. Therefore, iCLM4 incorporates a nonsteady leaf water model in the style of *Dongmann et al*. [1974], under the assumption that the leaf water volume does not change, but the isotopic ratio of leaf water tends toward steady state at a rate given by the ratio of the transpiration flux to the leaf water volume. Upon writing the budget equation and integrating analytically, the resulting mass balance resembles an exponential relaxation toward isotopic steady state:

$$R^i(t+\Delta t) = e^{-\Delta t/\tau}(R^i(t) - R^{*i}(t+\Delta t)) + R^{*i}(t+\Delta t). \tag{26}$$

The rate constant τ is determined by the ratio of the transpiration rate to the assumed constant specific leaf water volume; t is time; $R^i(t)$ and $R^i(t+\Delta t)$ are the modeled isotope ratios for the previous and current time steps, respectively; and $R^{*i}(t+\Delta t)$ is the isotope ratio at steady state for the current time step. The modeled value R^i is a weighted average between its value at the previous model time step and the newly calculated value in isotopic steady state, R^{*i}.

While numerical calculations are performed with isotope ratios and isotopologue mass, results are reported in the standard "delta" notation. Delta values (in permil, ‰) are calculated as

$$\delta_i = \left(\frac{R_i}{R_{SMOW}} - 1 \right) * 1000\,‰, \tag{27}$$

where R_i is the sample molar ratio of abundances of the heavy isotope ($H_2^{18}O$ or HDO) to the light isotope ($H_2^{16}O$) and R_{SMOW} is this ratio for standard mean ocean water. Model state variables are scaled by R_{SMOW} within the model code to provide the numerical advantage that the bulk water and water isotopic tracers have similar numerical precision. Deuterium excess, d, is calculated as

$$d = \delta D - 8 * \delta^{18}O. \tag{28}$$

3. Data and Simulations

3.1. Site-Level Comparisons

3.1.1. Data From Boulder Atmospheric Observatory

The site-level observational data consist of meteorological, hydrological, and water isotopic data spanning from May 2011 to September 2015 in Erie, Colorado, USA, approximately 25 miles north of Denver, Colorado. Measurements described here focus on those made from a 10 m tall tower at the Boulder Atmospheric Observatory site (BAO, 40°03′00″N, 105°00′14″W, 1584 m elevation). This is a semiarid grassland with minimal undergrowth and a canopy height of roughly 0.5 m. The BAO site was selected for this study due to the high quality and volume of available stable water isotopic data and previously validated hydrological and flux data.

Air temperature (°C) and humidity (%) were measured by a series of Vaisala HMP155 probes. Wind speed (m s^{-1}), ambient pressure (hPa), and concentrations of CO_2 (flux, μmol m^{-2} s^{-1}) and H_2O (mmol mol^{-1}) were measured using a Campbell Scientific EC150 open-path analyzer. Eddy covariance methods were used to determine latent and sensible heat fluxes (W m^{-2}). Upward and downward longwave and shortwave radiation (W m^{-2}) were measured using a suite of Kipp and Zonen CNR4 radiometers. Soil temperature and moisture measurements were gathered using Campbell Scientific and CS616 probes, respectively. Measurements of isotopic ratios of water vapor were made using a Picarro L2120-i water isotopic analyzer.

Measurements for the humidity, temperature, wind speed, and atmospheric pressure forcings were made at 1 min intervals and averaged to half-hourly intervals to match the model time step. Precipitation was measured at 1 min intervals and aggregated to half-hourly intervals. Water isotope ratios in vapor were measured at eight heights in a vertical that spans from 0.5 to 300 m, and values were obtained by measuring each height for 15 min. A continuous half-hourly time series to force the model was obtained by interpolating in time. Precipitation isotope ratios were collected at BAO at irregular intervals, with mean time between observations of 9.75 days (median is 7 days). Isotope ratios in precipitation water are assumed to be constant between measurements, which does not affect the simulation when there is no precipitation.

Between May 2011 and May 2012, isotope ratios of above-canopy water vapor and precipitation were missing from the forcing data. As a proxy, monthly measurements of isotope ratios in precipitation, collected in nearby Boulder, Colorado, were used for this time period [*International Atomic Energy Agency* (*IAEA*), 1994a]. Isotope ratios of atmospheric water vapor were assumed to be in isotopic equilibrium with the precipitation, at the measured atmospheric temperature [*Horita and Wesolowski*, 1994].

The simulations for BAO were initialized using observational data from the first date of the model simulations (11 May 2011). Initial soil temperature, moisture, and water isotopic profiles were linearly interpolated from data. Model results from May 2011 to May 2012 were used for spin-up, and results May 2012 to September 2015 were used for analysis. Only the growing season (May–October) was used for analysis because the most complete data sets (soil water isotope profiles, in particular) were available for the growing season.

3.1.1.1. Uncertainty Estimation

To provide a level of agreement which can reasonably be expected between the isotope ratios modeled by iCLM4 and those observed at BAO, the spatial representation (σ_{rep,δ_i}) and observational (σ_{obs,δ_i}) uncertainties for the site were estimated for soil water, water vapor, and ET source water (Keeling plot-based observations).

Samples of precipitation were collected at a network of four schools located throughout the Colorado Front Range region (representing an area approximately the same size as the BAO footprint in CLM4). The assumption is made that the spatial uncertainty in isotope ratios in precipitation serves as an indicator of the spatial uncertainty in soil water isotope ratios. Spatial uncertainty was estimated as the sample standard deviation of the difference between long-term averages of the isotope ratios of each site's precipitation and the isotope ratios of precipitation measured at BAO, yielding $\sigma_{rep,\delta^{18}O_{soi}} = 1.449\,‰$ and $\sigma_{rep,\delta D_{soi}} = 11.902\,‰$. These data are provided as supporting information. Observational uncertainties in soil water isotope ratios were derived from *Wassenaar et al*. [2014] (c.f., their Table 6). Accuracies were 0.075 ‰ for δ^{18}O and 0.550 ‰ for δD; precisions were 0.04 ‰ for δ^{18}O and 0.4 ‰ for δD. Combining these in quadrature with the spatial uncertainties yield $\sigma_{\delta^{18}O_{soi}} = 1.45\,‰$ and $\sigma_{\delta D_{soi}} = 11.9\,‰$. These errors, assuming independence between isotopic species, propagate to $\sigma_{d_{soi}} = 16.6\,‰$. It is important to note that these observational errors in isotope ratios are dominated by spatial heterogeneity, not analytical uncertainty.

Uncertainties in the Keeling plot-derived ET flux isotope ratios were calculated following the methods of *Good et al*. [2012]. It is expected that these estimates of uncertainty at the upper-most vapor inlet incorporate all spatial uncertainty, but this decreases with decreasing height along the tower. The representation uncertainty measured closer to the surface is much larger, and was estimated to be equal to $\sigma_{rep,\delta_{i,soi}}$. The uncertainty associated with the water vapor isotopic ratios at a given inlet height was estimated by fitting for each isotopic species *i* an exponentially decreasing function of the form

$$\sigma_{vap,i}(h) = A_i + B_i\, e^{-h/h_{\max}}, \tag{29}$$

where *h* is height (m) A_i and B_i are parameters determined by fitting this function to the requirements $\sigma_{vap,i}(0) = \sigma_{rep,\delta_{i,soi}}$ and $\sigma_{vap,i}(h_{\max}) = 0$, and h_{max} is the height of the uppermost inlet (8.5 m). This spatial uncertainty was added in quadrature to the observational uncertainties associated with each vapor isotopic measurement, estimated as above from *Wassenaar et al*. [2014]. This total uncertainty at each inlet was factored into the calculations following *Good et al*. [2012] to find the total observational and spatial uncertainties in ET flux isotope ratios to be $\sigma_{\delta^{18}O_{ET}} = 2.85\,‰$ and $\sigma_{d_{ET}} = 15.1\,‰$. These error estimates were calculated at a daily time scale.

3.1.1.2. Soil Moisture Data Assimilation

An experiment was conducted to evaluate the extent to which the native CLM4 soil hydrological scheme is principally responsible for biases in the modeled soil water isotope ratios relative to observations. Soil moisture data were assimilated into the BAO model simulation at each time step and soil layer (*j*) using a one-dimensional basic linear Kalman filtering approach [*Kalman*, 1960; *Rodgers*, 2000]. A zero flux boundary condition was imposed at the bottom of the iCLM4 soil column. Based on the change in water content of each soil layer ($\theta_{new,j} - \theta_{old,j}$), starting with the lowest layer (j_{max}), a flux between layers *j* and $j - 1$ was calculated. Using the forecast isotopic ratios of each soil layer, the isotopic fluxes during each assimilation step were calculated, and the water isotopic composition of each soil layer was updated. In effect, this data assimilation approach is a "nudging" of the model state toward the observed soil moisture state, where the strength of the nudging is determined by the uncertainties in the model and observations. This soil moisture data assimilation method does not conserve soil moisture. Rather, an "assimilation flux" at the soil surface results, and may be viewed as an error term in the surface soil moisture balance. This error term is the result of poor constraint on precipitation, surface runoff, subsurface runoff, and infiltration fluxes.

3.1.2. Results From Boulder Atmospheric Observatory

3.1.2.1. Latent and Sensible Heat Fluxes

Figure 2 shows the modeled surface latent heat and sensible heat fluxes plotted against the observations of these fluxes from BAO derived from eddy covariance, averaged on a daily time scale. A low model bias in latent heat flux was present (3.1 W m^{-2}, Figure 2a). Sensible heat flux displayed a high model bias of 27.0 W m^{-2} (Figure 2b). These results reflect model structural errors which are inherent in the original, nonisotopic, version of CLM4. These errors will propagate into the isotopic evapotranspiration terms in the water isotopic hydrology in iCLM4. A more comprehensive investigation of the uncertainties in the surface fluxes modeled by CLM4 should be undertaken, but within the scope of the present study, the sensitivity of modeled isotope ratios to errors in the bulk soil moisture reveal the value of using the isotopic observations for diagnosing errors in water transport.

3.1.2.2. Isotope Ratio Estimates

While the total latent heat flux displays biases (Figure 2a), it is useful to compare the isotope ratios of the evapotranspiration (ET) flux against those derived from observations of humidity, isotope ratios of water vapor, and Keeling plot techniques [*Keeling*, 1958].

For BAO, the modeled isotope ratio $\delta^{18}O$ and deuterium excess *d* of the ET flux were biased high by 2.37 ‰ and 16.7 ‰, respectively (Figures 3a and 3b). These biases were calculated from daily averages of Keeling plot-derived isotope ratios of ET fluxes for observations and directly from model output (cf. section 2.1.2). While these biases appear large at first glance, the estimates of observational uncertainties were also large, at 2.85 ‰ for $\delta^{18}O$ and 15.1 ‰ for *d* (section 3.1.1.1). The modeled water vapor isotope ratios at two meters height were in good agreement with observations. This was to be expected from simulations for a site for which 2 m is above the (0.5 m) canopy.

3.1.2.3. Soil Moisture

The modeled soil moisture profile and isotope ratios of $\delta^{18}O$ and *d* for BAO highlight model hydrology shortcomings and strengths (Figure 4). Observations are displayed as scatter points with the color of

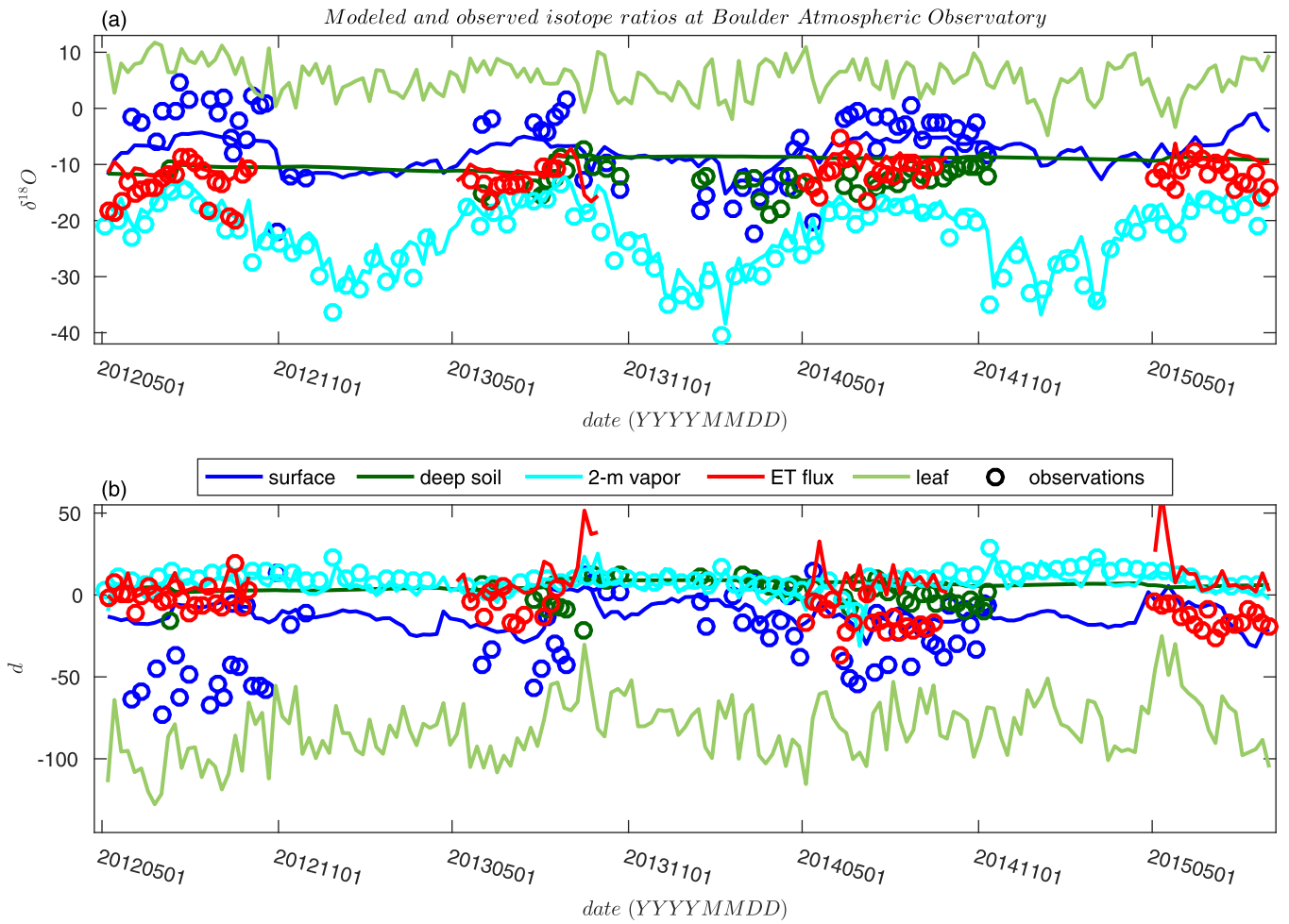

Figure 3. Comparison between modeled and observed isotope ratios (a) $\delta^{18}O$ and (b) deuterium excess, *d*, of ET flux for BAO. Included are isotope ratios of surface soil water, soil water at 0.85 m depth, leaf water, water vapor at 2 m height, and ET flux.

shading corresponding to the colors of the contours, which represent the modeled moisture and isotope ratio profiles. Note that the modeled bulk soil water profiles are the result of the hydrology native to nonisotopic CLM4, and the isotopic physics introduced in the present work have no impact on those results. A first estimate of the model biases attributable to the bulk soil moisture may be obtained by examining the errors in soil water isotope ratios in the control versus the bulk soil moisture assimilation experiments. Thus, it is immediately evident that many of the shortcomings in the isotopic simulation arise from poor simulation of the base model water balance. This serves as an excellent reminder of the value of isotopic measurements in diagnosing the origin of model-observation mismatch.

During 2012 and summer 2013, the modeled soil moisture profile exhibited the summer drying and fall/winter wetting displayed by the observations (Figures 4a and 4b). Major precipitation events do not show infiltration as deeply into the soil as observations suggest. A particular example is in association with a major flooding event that occurred in the Colorado Front Range in September of 2013. During this event, the region experienced precipitation totals up to about 450 mm over a 10 day period, and significant standing water in low elevation regions [*Yochum*, 2015]. For example, the spring 2013 rainfall does not inject as deeply into the modeled soil moisture simulation ($<$10 cm) as seen in the observations (about 10$-$50 cm) (Figures 4a and 4b). This demonstrates that the modeled connectivity of the near-surface soil moisture to the deeper soils is not as strong as seen in the available data.

This issue of too weak of a hydrological connectivity between surface and deeper soils was also seen in the modeled isotopic moisture profiles. For example, in the year from November 2013 to November 2014, the

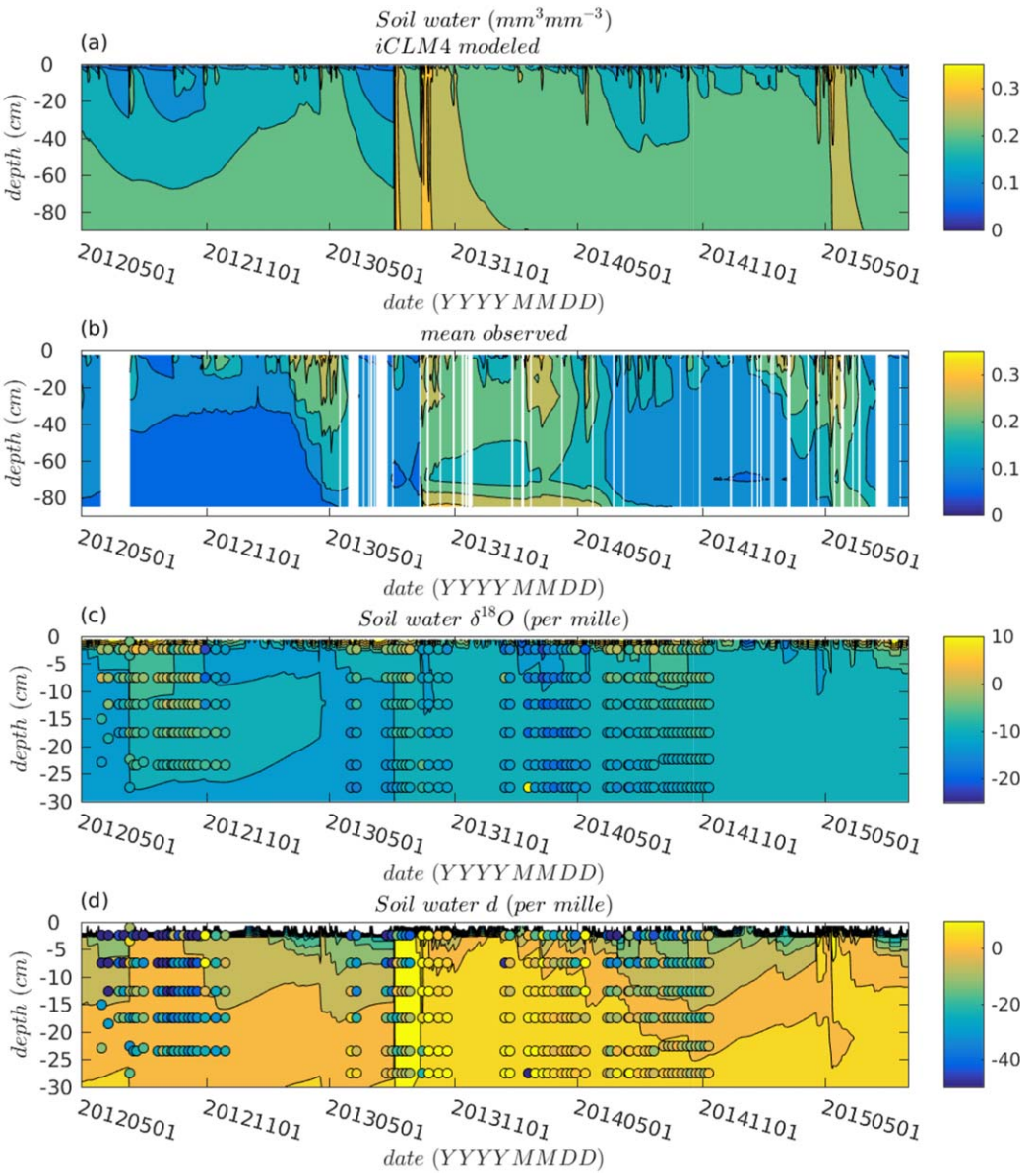

Figure 4. Comparison between (a) modeled and (b) observed bulk soil water ($mm^3\ mm^{-3}$) and its (c) isotope ratio, $\delta^{18}O$, and (d) deuterium excess, *d*, for BAO.

modeled deuterium excess *d* in soil water showed overall consistency with the observed magnitude of deuterium excess, but the model generally underestimated the depth to which the evaporative enrichment in $\delta^{18}O$ and decrease in deuterium excess extends (Figure 4d). Specifically, in May 2014, a deuterium excess of about $-10‰$ was observed at 12.5 cm depth, but in the modeled profile, $-10‰$ deuterium excess was at about 3 cm depth. Similarly, the evaporative enrichment in $\delta^{18}O$ during summer and early fall 2014 extends to about 10 cm depth, but in October 2014 the model missed the observed enrichment (Figure 4c). On average, however, the summer enrichment and winter depletion of $\delta^{18}O$ were present and matched the measured isotope ratios with a mean growing season bias of $-0.32‰$ (Figure 4c). The model biases are defined as *model-observations*. The modeled *d* in soil water was too positive during the growing season (mean bias of $18.4‰$), and in the 2012–2013 season, lacked the precise seasonal cycle and depth of evaporative decrease of *d* in the summers and increase in winters (Figure 4d). From this control simulation at BAO, it is clear that the modeled soil water isotope ratios were qualitatively accurate, but conclusive statements regarding the soil water isotopic scheme cannot be made because of potentially confounding inherent errors in the bulk soil water hydrology in CLM4.

To alleviate this limitation, soil moisture data were assimilated according to the experiment described in section 3.1.1.2 using data from the BAO site, yielding a close match between modeled and observed soil water content, as expected (Figures 5a and 5b). For growing season (May–October) months, the mean model bias in bulk soil water was reduced from 0.0182 $mm^3\ mm^{-3}$ to $-0.0038\ mm^3\ mm^{-3}$. As a consequence of the improved simulation of bulk soil water, modeled soil water isotope ratios also slightly better matched observations. Soil water $\delta^{18}O$ shows greater seasonality at depth, and displays a slight improvement in column mean growing season bias from $-0.32‰$ to $-0.31‰$ and root-mean-squared error (RMSE) from 3.55‰ to 3.30‰ ($\sigma_{\delta^{18}O_{soi}} = 1.45‰$; Figures 5c and 6a). The simulation of deuterium excess *d* was improved as well, reducing the model bias of 18.4‰ to 12.4‰ and RMSE from 23.9‰ to 20.5‰ ($\sigma_{d_{soi}} = 16.6‰$; Figure 5d). Further improvements were seen specifically in the deep (0.85 meter) soil water *d*; this bias was reduced from 7.0‰ to −0.1‰ (Figures 5d and 6b). During the November 2013 to November 2014 year, the trend toward soil moisture *d* depletion at depth is much better matched in the assimilation experiment (bias of 12.9‰, RMSE is 17.8‰; Figure 5d) than the control (bias of 17.6‰, RMSE is 21.8‰; Figure 4d).

In summary, the native CLM4 bulk soil moisture simulation was "nudged" into better agreement with observational data, and the simulated water isotope ratios reflected the adjusted vertical flux of soil water that was implied by the bulk moisture transport from this data assimilation. As a result of the (forced) improvement in the bulk soil moisture simulation, the resulting soil water isotope ratios were also in better agreement with the observational data. Even after the assimilation, however, there remains some mismatch between the modeled and observed soil water isotopic profiles. While it is not expected that the model will reproduce the observations exactly (due to observational and model structural uncertainties), other potential sources of error include a lack of subsurface water vapor transport and potential heterogeneity in soil characteristics. Additionally, this assimilation approach only corrects the soil moisture amount, and does not adjust the fluxes themselves.

3.2. Impact of Land Processes in Climate *Simulations*

3.2.1. Global-Scale Experiments

An investigation of the model sensitivity to individual isotopic kinetic effects' parameterizations used on a global scale is presented, in order to gain insight into how these kinetic factors may best be chosen. In a coupled model framework, the surface and subsurface runoff in CLM4 flows into the river model component of the NCAR Community Earth System Model (CESM), the River Transport Model (RTM) [*Hurrell et al*., 2013]. Evapotranspiration couples the land surface to the atmospheric component of CESM, the Community Atmosphere Model, version 5 (CAM5), which precipitates back to the land surface, and impacts the land surface through the above-canopy humidity as well. The isotopic land surface model detailed in the present work was coupled to isotope-enabled versions of RTM (iRTM) and CAM5 (iCAM5) [*Nusbaumer et al*., 2017]. iRTM is structured such that river outflow from iCLM4 is transported to oceans, preserving water isotope ratios. In the present work, the coupled land-river-atmosphere model is hereafter referred to as "iCESM," although it should be noted that ocean and dynamic sea ice models were not active in this setup.

A spin-up simulation was run from 1850 to 1975. Isotope ratios of vegetation leaf and xylem water, soil water, and canopy water vapor were initialized at values derived from long-term averages from the Global Network of Isotopes in Precipitation (GNIP) [*International Atomic Energy Agency* (*IAEA*), 1994a]. This simulation used the parameterizations outlined in section 2.1, at 2° resolution. A series of experiments conducted to investigate the sensitivity of the modeled climate system to the land surface water isotopic parameterizations is described below, and summarized in Table 1. Each simulation was branched from the spin-up simulation in 1975 and ran until 2015 with the modifications specified. The first 20 years (1975–1995) of each experiment were discarded as spin-up; the last 20 years (1995–2015) of each experiment were used for analysis, their mean isotope ratios serving as an estimate of long-term average climate behavior. A control experiment ("EC") used the same land surface kinetic fractionation setup as the spin-up simulation, with the exception that parameterization (M78) was used for the surface evaporative kinetic effect instead of (MJ79), in agreement with other, similar models [*Buenning et al*., 2014; *Rothfuss et al*., 2010; *Xu et al*., 2008; *Williams et al*., 2004; *Roden et al*., 2000; *Wang and Yakir*, 2000]. In experiment E0, all land surface water isotopic fractionation factors were neglected. In experiment ELI, a kinetic fractionation factor following (M78) with $n = 1$ was assigned to model diffusive transport within the litter layer. Experiment ES changed the kinetic fractionation factor associated with surface evaporation from (M78) to (MJ79). (MJ79) was offered as the alternative

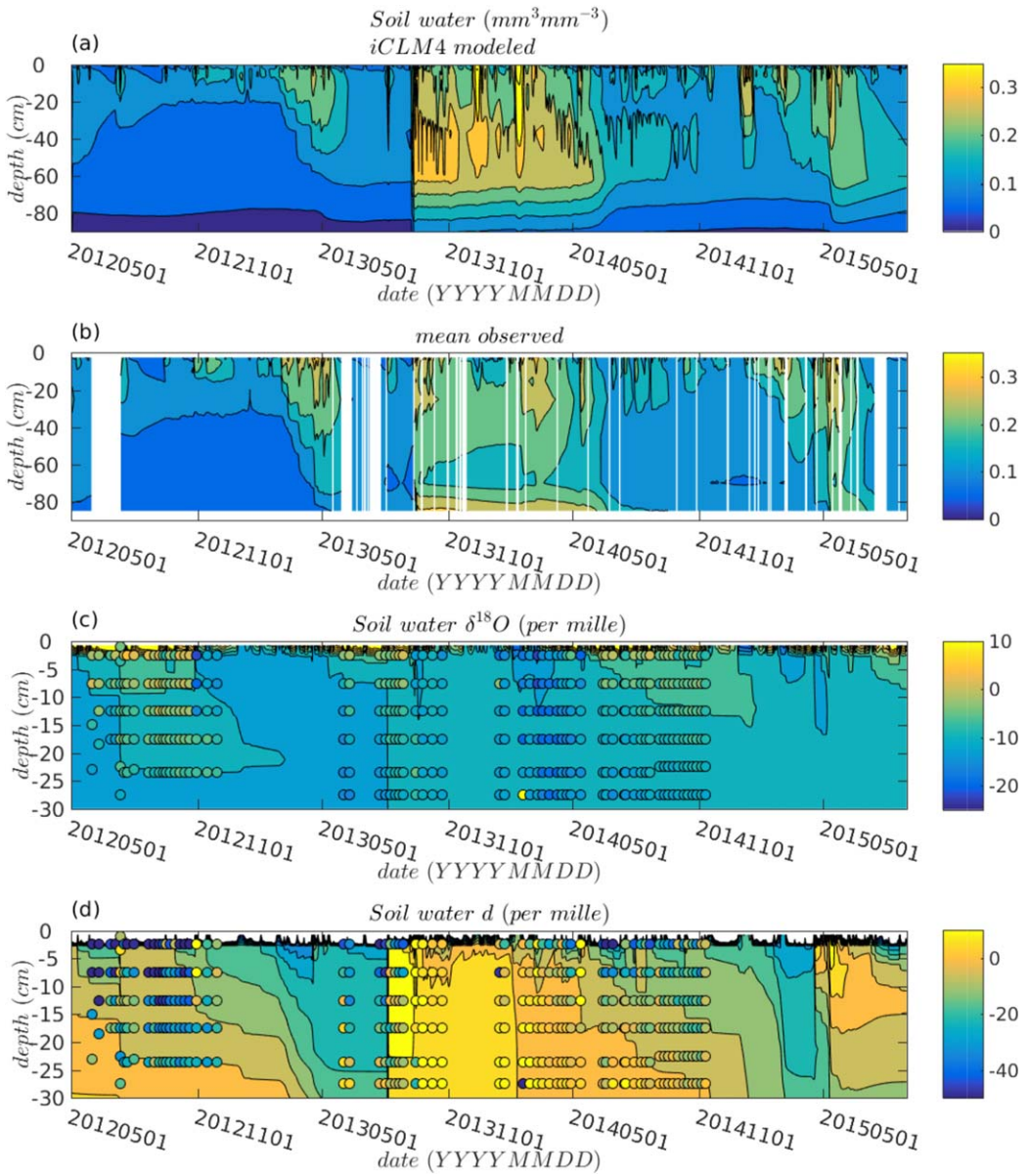

Figure 5. Comparison between modeled and observed bulk soil water (mm^3 mm^{-3}, (a) and (b), respectively) and its (c) isotope ratio, $\delta^{18}O$, and (d) deuterium excess, *d*, for BAO. These simulations are identical to those in Figure 4, but have bulk soil moisture data assimilated using a Kalman filter approach.

in ES because (1) (MJ79) yields a typically weaker kinetic effect, making ES a complementary experiment to ELI, and (2) (MJ79) makes explicit the dependence of the kinetic effect on turbulent conditions through the friction velocity and Reynolds number.

Due to errors and biases in the iCAM5 and iRTM schemes, it is not expected that changing the land surface scheme alone will remove errors relative to global isotope ratio data sets. A set of experiments were conducted to examine the impacts of the sensitivity experiments outlined in Table 1 on the soil moisture isotopic simulation at the BAO site. These tests suggested that, in light of the biases inherent in running a global climate model, the precise form of the land surface kinetic fractionation is essential to obtain a high quality water isotopic simulation (see supporting information, Figures S8 and S9). Investigations into the atmospheric processes involved are treated in detail in *Nusbaumer et al.* [2017]. Here experiments are designed to evaluate the importance of the land surface parameterizations by analyzing the coupled climate model response, and provide a starting point for future work using iCLM4.

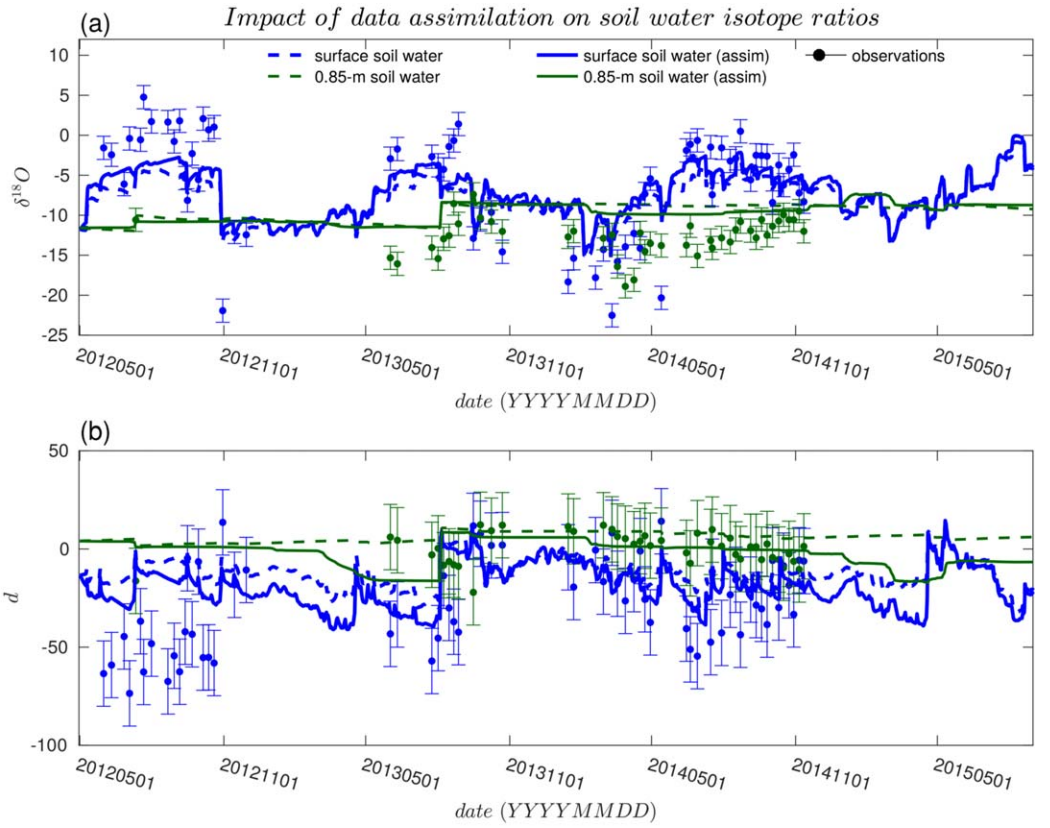

Figure 6. Comparison between modeled and observed soil water isotope ratios (a) δ^{18}O and (b) deuterium excess, *d*, when bulk soil moisture was assimilated using a Kalman filter.

After the runs were completed an error in the treatment of different plant types was found that has a small (positive) bias on the deuterium excess. Since the impact was confined to the high northern latitudes, with opposing tendencies in summer versus winter, and the impact on a single isotope ratio was small, the error has trivial impact on the results reported here. This error has since been fixed in the available source code.

3.2.2. Global-Scale Data

3.2.2.1. GNIP

In iCESM, modeled isotope ratios in precipitation were compared to isotope ratios from the Global Network of Isotopes in Precipitation (GNIP) [*International Atomic Energy Agency* (*IAEA*), 1994a]. Additional stations were added from studies in the Maritime Continent [*Moerman et al*., 2013; *Kurita et al*., 2009] region as well, in order to improve the spatial coverage of isotopic precipitation stations globally. Raw GNIP data were processed as in *Buenning et al*. [2014] to obtain a gridded global climatology.

For the other global comparisons, the mean iCESM/GNIP precipitation isotope ratio bias was subtracted to remove a known systematic error that otherwise complicates the present analysis of land surface influences. Thus, the results presented are normalized to account for the iCESM model bias in precipitation relative to the GNIP observations. Specifically, the figures that follow show $\delta_{data}-\delta_{GNIP}$ versus $\delta_{iCLM4}-\delta_{iCAM5}$, where δ_{data} is the river or vegetation isotope ratio from a global data set, δ_{iCLM4} is the isotope ratio modeled by iCLM4 matching the river or vegetation isotope ratios, δ_{iCAM5} is the precipitation isotope ratio modeled by iCAM5, and δ_{GNIP} is the precipitation isotope ratio from GNIP.

3.2.2.2. GNIR

The iCESM sensitivity experiments produced output for isotope ratios of river flow throughout river basins, as well as inflow to oceans. These modeled river isotope ratios from iRTM represent an integrated ratio, incorporating iCLM4 surface and subsurface runoff along the flow path. This is commensurate with the isotope ratios measured by the Global Network of Isotopes in Rivers (GNIR) [*International Atomic Energy Agency* (*IAEA*), 2012; *Vitvar et al*., 2007], which span 1967–2015.

Table 1. Global Isotope-Enabled Model Experiments

	Equilibrium Fractionation	Surface Evaporation	Canopy Evaporation	Transpiration	Nonsteady Leaf	Peclet	Litter
EC	Yes	(M78)	(M78)	Equations (10) and (11)	Yes	Yes	No
E0	No	No	No	Steady	No	No	No
ES	Yes	(MJ79)	(M78)	Equations (10) and (11)	Yes	Yes	No
ELI	Yes	(M78)	(M78)	Equations (10) and (11)	Yes	Yes	(M78)

3.2.2.3. MIBA

Observations of isotope ratios of leaf and xylem water from the network of Moisture Isotopes in the Biosphere and Atmosphere (MIBA) offer a constraint on the parameterizations of isotopic surface processes [*International Atomic Energy Agency* (*IAEA*), 1994b; *Twining et al*., 2006]. Raw MIBA data for isotope ratios in xylem water and leaf water were averaged for each site to obtain a long-term average climatology. Site information for the MIBA locations used here is provided in supporting information Data Set S2.

3.2.3. Results: Global Comparisons

3.2.3.1. Global Network of Isotopes in Precipitation

In the control sensitivity experiment (EC), iCESM produced isotope ratios δ^{18}O in precipitation which were too enriched in northern high latitudes and the Himalayas and too depleted in mid-latitudes and southern hemisphere (Figure 7a). By removing all surface isotopic effects, it was shown that the land surface alone was responsible for only a minor portion of errors, mostly over Africa and Asia (Figure 7b). Neither weakening (ES) nor strengthening (ELI) the surface kinetic effects relative to EC improved the low δ^{18}O bias (Figures 7c and 7d). Deuterium excess *d* was typically biased low in high latitudes (both northern and southern) and high in the tropics and subtropics (Figure 8a). Both experiments weakening the surface kinetic effect (E0 and ES) improved this *d* bias (Figures 8b and 8c), and strengthening the surface kinetic effect had mixed weak effects (Figure 8d). This highlights the need to correctly account for kinetic effects in ecosystems to produce realistic simulations of isotope ratios in continental regions. In Figures 7 and 8, the locations of GNIP observation sites are denoted with diamonds (◇). Note that in Figures 7 and 8, plot (a) shows the control model (EC) bias relative to GNIP, while plots (b–d) show the sensitivity simulation results relative to the control model, *experiment-control*.

Global mean biases (*model-observations*) for the sensitivity tests EC, E0, ES, and ELI for δ^{18}O were $-1.44‰$, $-0.84‰$, $-1.40‰$, and $-1.56‰$, respectively, and for *d* were $1.5‰$, $-0.9‰$, $0.9‰$, and $2.1‰$. The soil water isotope ratio uncertainty estimates for BAO were $1.45‰$ in δ^{18}O and $16.6‰$ in *d*, and were derived from precipitation data. The grassland environment at BAO is a more straightforward prospect than complications that arise in slopped terrain or where there is more complex ecosystem structure. Thus, it is expected that the first-order observational uncertainties (spatial and analytical) for BAO are representative of those associated with other sites. Therefore, it is unlikely that strengthening the surface kinetic effect beyond that of (M78) is appropriate on a global scale.

3.2.3.2. Global Network of Isotopes in Rivers

For both δ^{18}O and *d*, the modeled isotopic offset between the ratios in river outflow relative to precipitation is relatively insensitive to the precise form of the kinetic fractionation factor used for the surface evaporation (Figure 9). RMSE, mean iCESM bias, and correlation coefficient are given in each panel of Figure 9. This insensitivity demonstrates that biases and errors in the river water isotope ratios are likely attributable to water isotopic effects beyond those due to soil evaporation alone—for example, lateral transport of subsurface moisture, or subsurface vapor diffusion. Contour maps show little contrast between experiments due to the relative insensitivity of the river outflow isotope ratios to the specific land surface isotopic scheme used, reflecting the assertion that the land surface is near steady state with respect to the balance between precipitation, evapotranspiration, and runoff on long time scales.

3.2.3.3. Moisture Isotopes in the Biosphere and Atmosphere

Comparisons with MIBA leaf water isotope ratios highlighted the danger of neglecting land surface isotopic processes (Figure 10). The E0 experiment which, to test the importance of land fractionation, ignored these processes, incurred extremely large biases in leaf water isotope ratios relative to the isotope ratios in precipitation: $-17.6‰$ in δ^{18}O and $65.9‰$ in *d*. We use uncertainties in soil water isotope ratios to estimate the uncertainties in leaf water isotope ratios. As we are concerned primarily with long-term averages and soil water serves as vegetation source water, these are an appropriate estimate. The modeled leaf water δ^{18}O

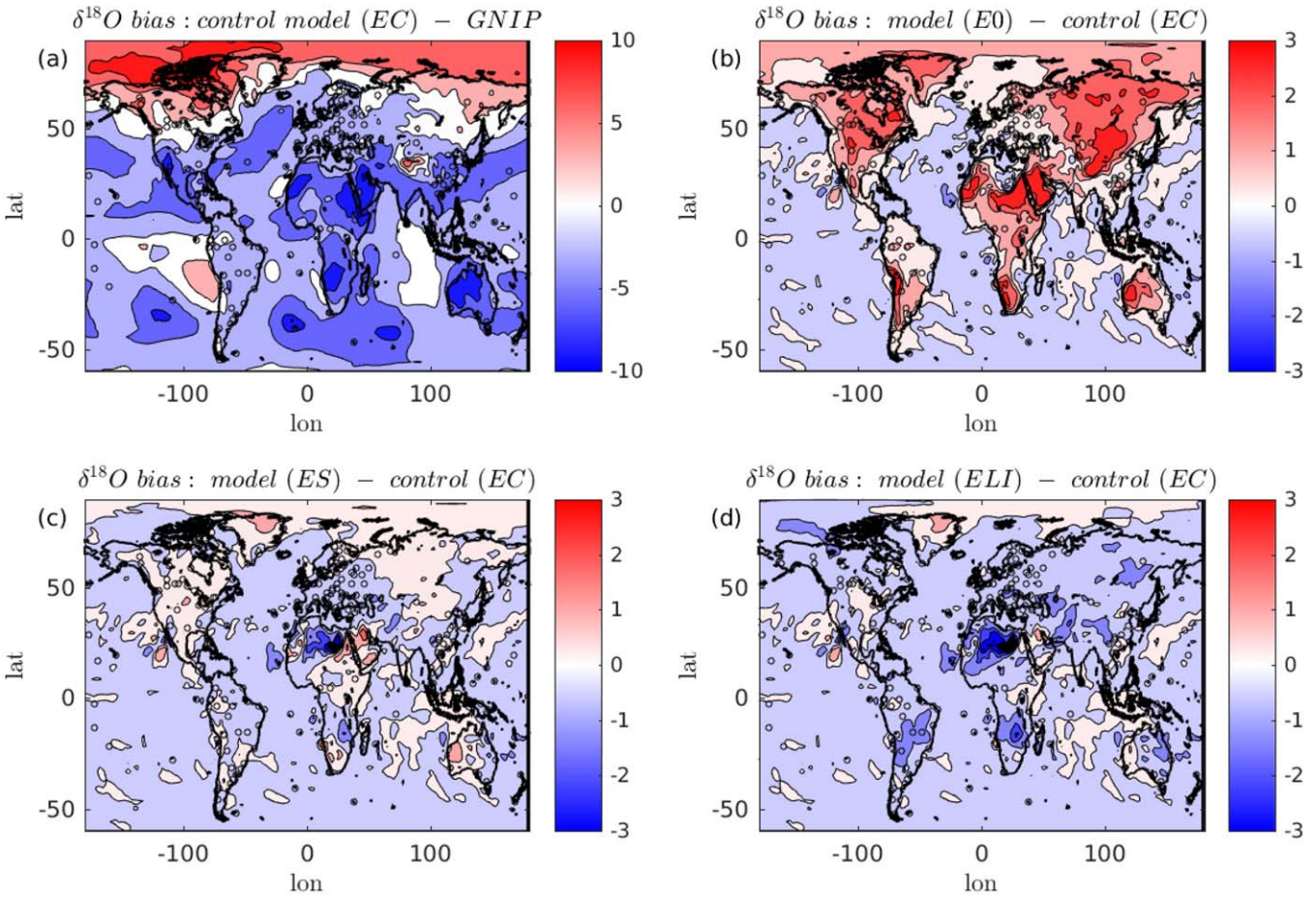

Figure 7. Biases of iCESM-modeled δ^{18}O of precipitation (a) relative to GNIP observations for EC, and relative to the control experiment for the sensitivity experiments (b) E0, (c) ES, and (d) ELI. Contours represent (a) *model-observations* bias and (b, c, and d) *model-control* bias. Locations of GNIP observation sites are denoted with a diamond (◇).

bias with respect to the MIBA observations was within this uncertainty estimate, pointing to decent agreement in the three experiments accounting for isotopic fractionation effects (Figure 10). All displayed similar biases in leaf water *d*, which is attributed to poor constraint on the isotopic kinetic fractionation factors through stomata and the leaf boundary layer (equations (21) and (22)). The vegetation and aerodynamic resistances to heat and moisture transport (equations (21)–(23)) partly control the strength of these kinetic effects. In practice, a parameter calibration approach for these ecosystem resistances and other factors related to the water isotopic kinetic effects could be implemented, which will be the focus of a follow-up study.

Xylem water isotope ratios also underscored the importance of accounting for land surface isotopic processes (Figures 11b and 11f). From the δ^{18}O comparisons via scatter plots (Figures 11a–11d) and contour maps (Figure 12), experiments ELI and EC displayed the best agreement with MIBA observations. All experiments overestimated the observed depletion in xylem water relative to precipitation at higher northern latitudes, but the control EC and experiment ELI demonstrate how calibrating the strength of the kinetic fractionation may serve to mitigate this bias. Modeled *d*, however, showed that the surface evaporative kinetic effect parameterized by (M78) was too strong in mountain and desert regions (Figures 13a and 13d) but a parameterization following (MJ79) yields good agreement (Figure 13c). These highly depleted isotope ratios in vegetation water were confined to regions with low LAI (primarily mountain and desert regions) and areas with little/no observational data to constrain model results. This arises from low amounts of bulk water is these regions (e.g., the Sahara). When evaporation occurs, the isotopic kinetic separation still enriches the soil water in heavier isotopes relative to lighter ones,

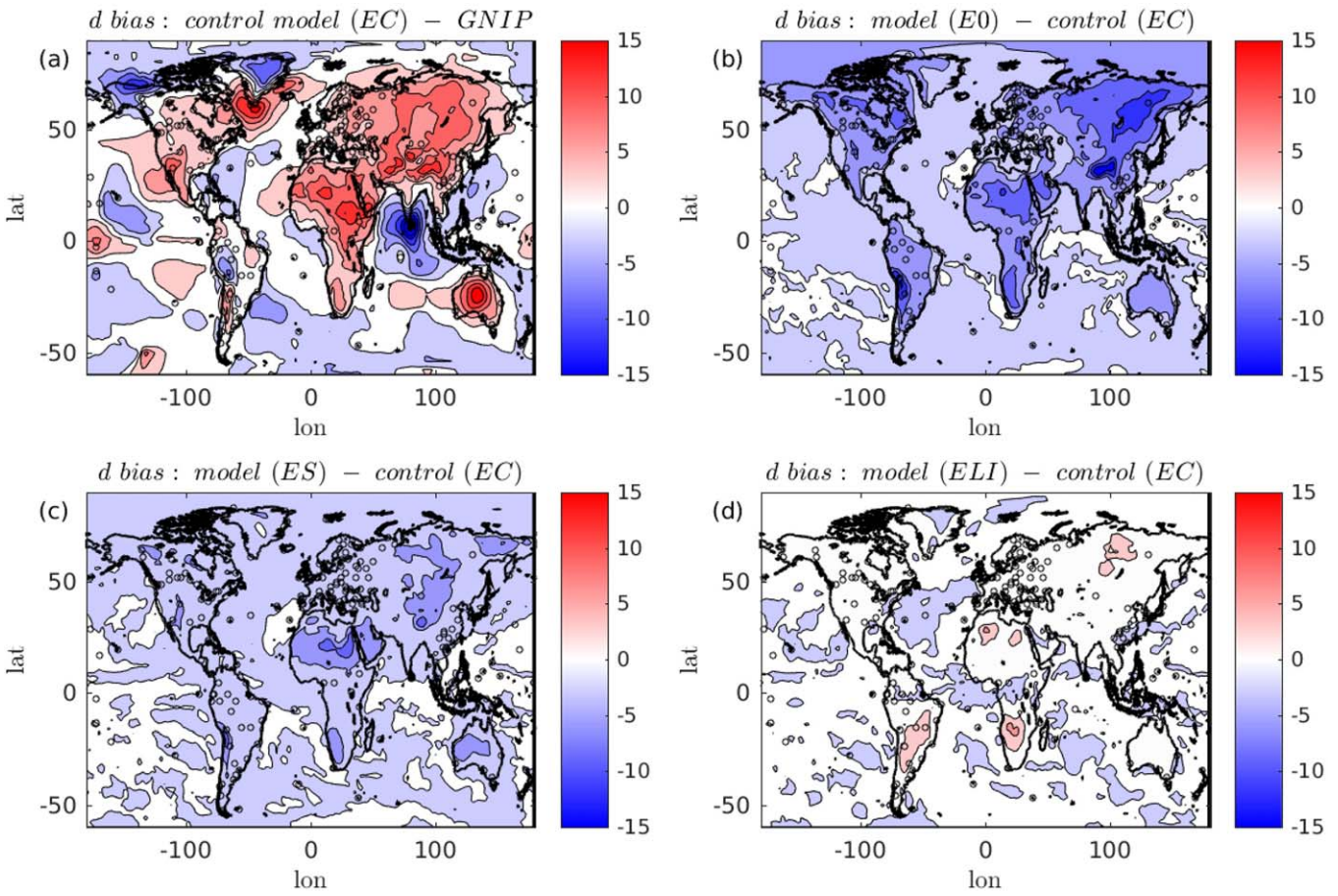

Figure 8. Biases of iCESM-modeled *d* of precipitation (a) relative to GNIP observations for EC, and relative to the control experiment for the sensitivity experiments (b) E0, (c) ES, and (d) ELI. Contours represent (a) *model-observations* bias and (b, c, and d) *model-control* bias. Locations of GNIP observation sites are denoted with a diamond (◇).

even though the total amount of moisture available has decreased. Thus, the enrichment in $\delta^{18}O$ becomes quite large (Figures 12a and 12d) and the deuterium excess becomes quite small (Figures 13a and 13d).

4. Summary and Discussion

A water tracer scheme in CLM4 has been outlined and implemented, with particular attention given to applications in stable water isotope hydrology. The iCLM4 model has been forced with and validated against site-level observations from a field site in central Colorado, USA. iCLM4 was also run in a coupled, isotope-enabled modeling framework (iCESM), which was validated against global networks of observations of isotope ratios in precipitation, river outflow, and vegetation moisture.

Comparisons with long-term mean isotope ratios in precipitation (GNIP), river outflow (GNIR), and vegetation xylem and leaf water (MIBA) indicated that (M78) (experiment EC) or (M78) with an additional fractionation through the leaf litter layer (experiment ELI) were the most appropriate parameterizations for the kinetic effect during evaporation of surface water, on a global average scale. These experiments indicated that future work should consider calibrating the fractionating effects beyond those during surface soil evaporation—for example, through the leaf boundary layer and stomatal conductances, or by accounting for subsurface vapor diffusion. Indeed, the MIBA results revealed that (M78), despite being in common use [*Buenning et al*., 2014; *Rothfuss et al*., 2010; *Xu et al*., 2008; *Williams et al*., 2004; *Roden et al*., 2000; *Wang and Yakir*, 2000], strongly overestimates the magnitude of the kinetic isotopic effect for mountain and desert regions (Figures 13a and 13d). Therefore, (M78) is recommended, noting the caveats above. The global experiments and model-data comparison presented here comes with many caveats of its own, including

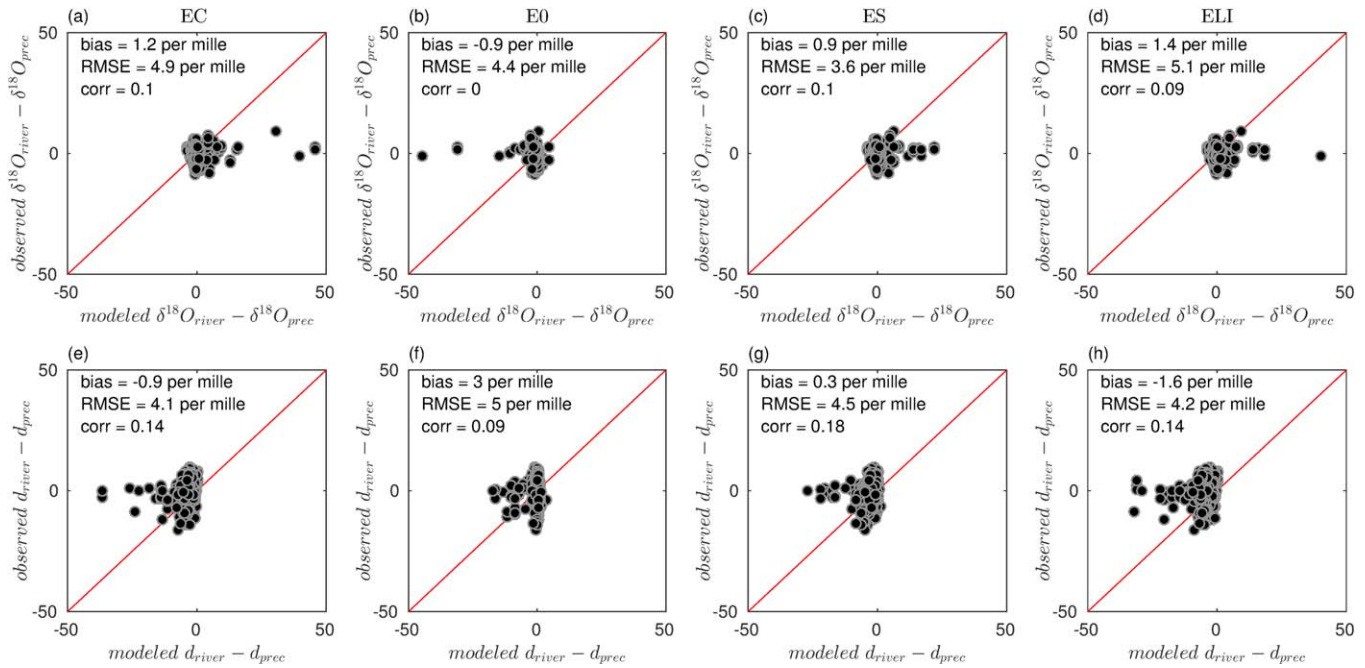

Figure 9. Comparison between iCESM-modeled and GNIR observations of δ^{18}O (top row) and deuterium excess, *d* (bottom row) in river outflow for the sensitivity experiments: (a and e) EC, (b and f) E0, (c and g) ES, (d and h) ELI. Modeled isotope ratios are relative to isotope ratios in iCAM5 precipitation and observed isotope ratios are relative to GNIP.

strong spatial heterogeneity, potential seasonal and local effects, imperfect representation of local vegetation covers, and the numerical uncertainty associated with using an interpolated GNIP data product.

The sensitivity of the vegetated land surface water isotopic signal to the specific form of the kinetic fractionation factor during evaporation is consistent with the results of *Haese et al*. [2013]. These authors also found

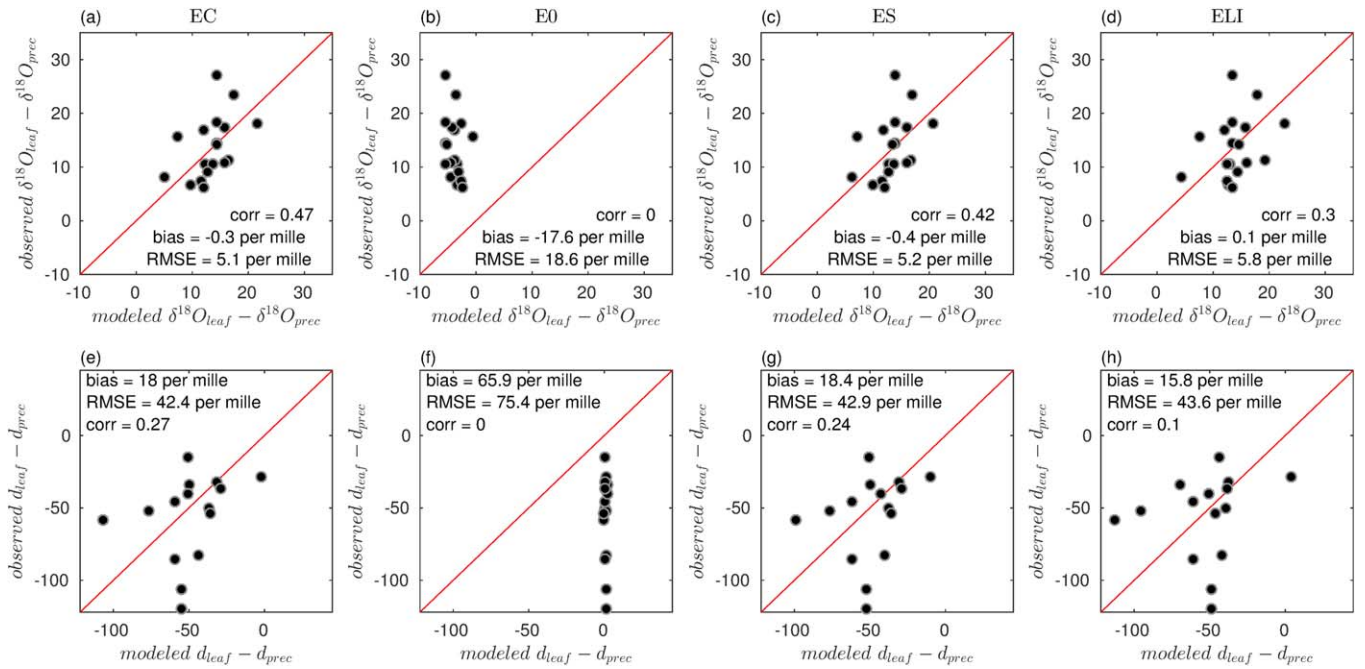

Figure 10. Comparison between iCESM-modeled and MIBA observations of leaf water δ^{18}O (top row) and deuterium excess, *d* (bottom row) for each sensitivity test: (a and e) EC, (b and f) E0, (c and g) ES, (d and h) ELI. Modeled isotope ratios are relative to isotope ratios in iCAM5 precipitation and observed isotope ratios are relative to GNIP.

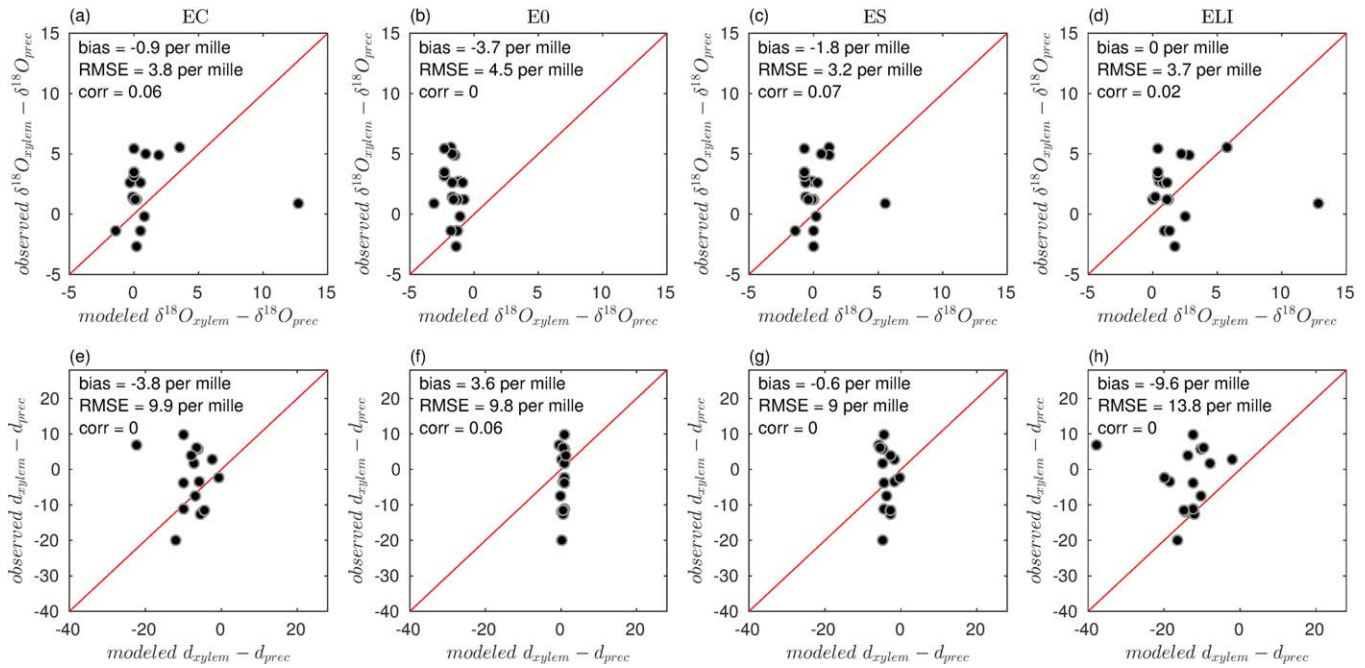

Figure 11. Comparison between iCESM-modeled and MIBA observations of xylem water δ^{18}O (top row) and deuterium excess, *d* (bottom row) for each sensitivity test: (a and e) EC, (b and f) E0, (c and g) ES, (d and h) ELI. Modeled isotope ratios are relative to isotope ratios in iCAM5 precipitation and observed isotope ratios are relative to GNIP.

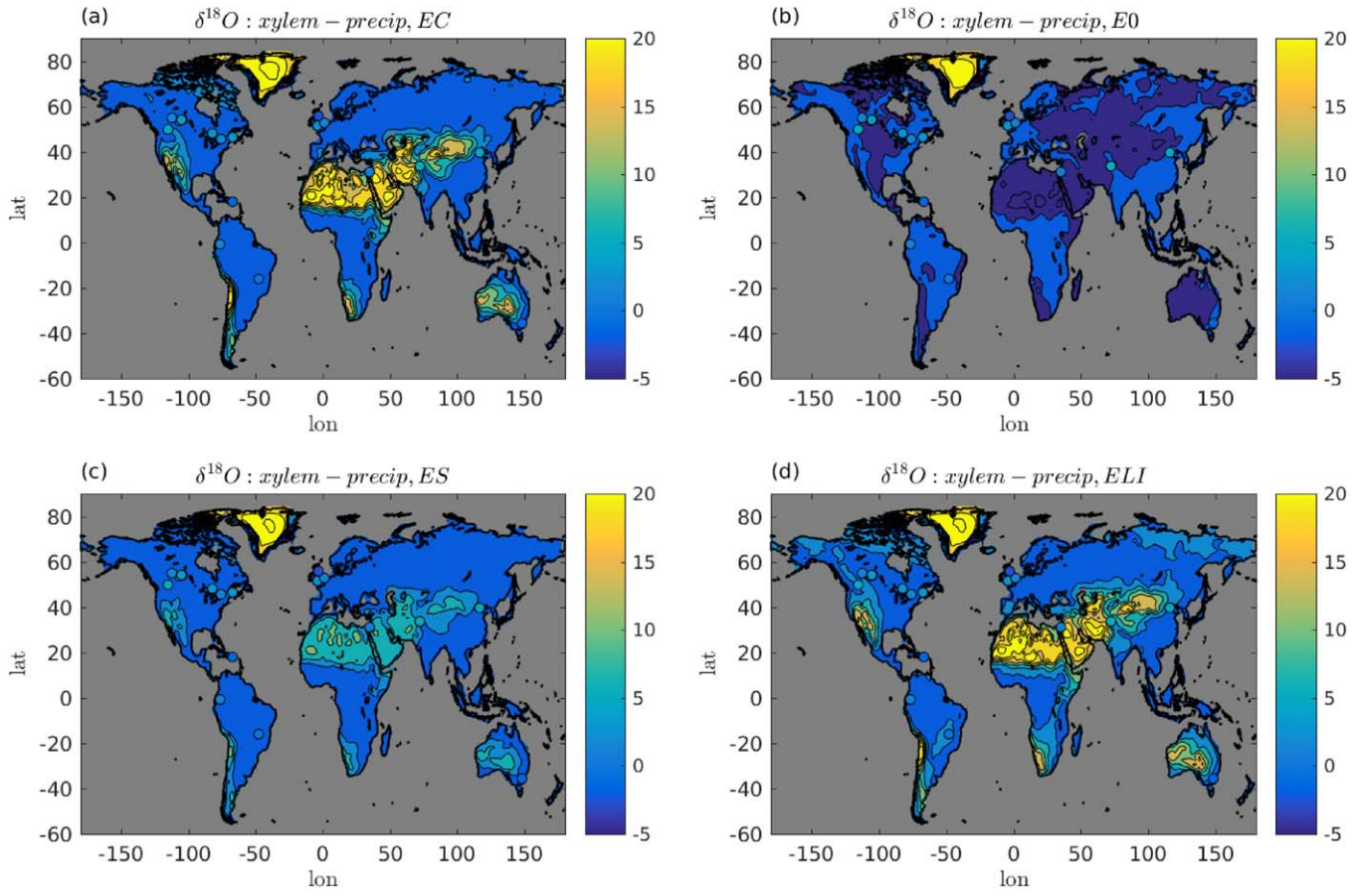

Figure 12. Comparison between iCESM-modeled and MIBA observations of xylem water δ^{18}O for the sensitivity experiments: (a) EC, (b) E0, (c) ES, and (d) ELI.

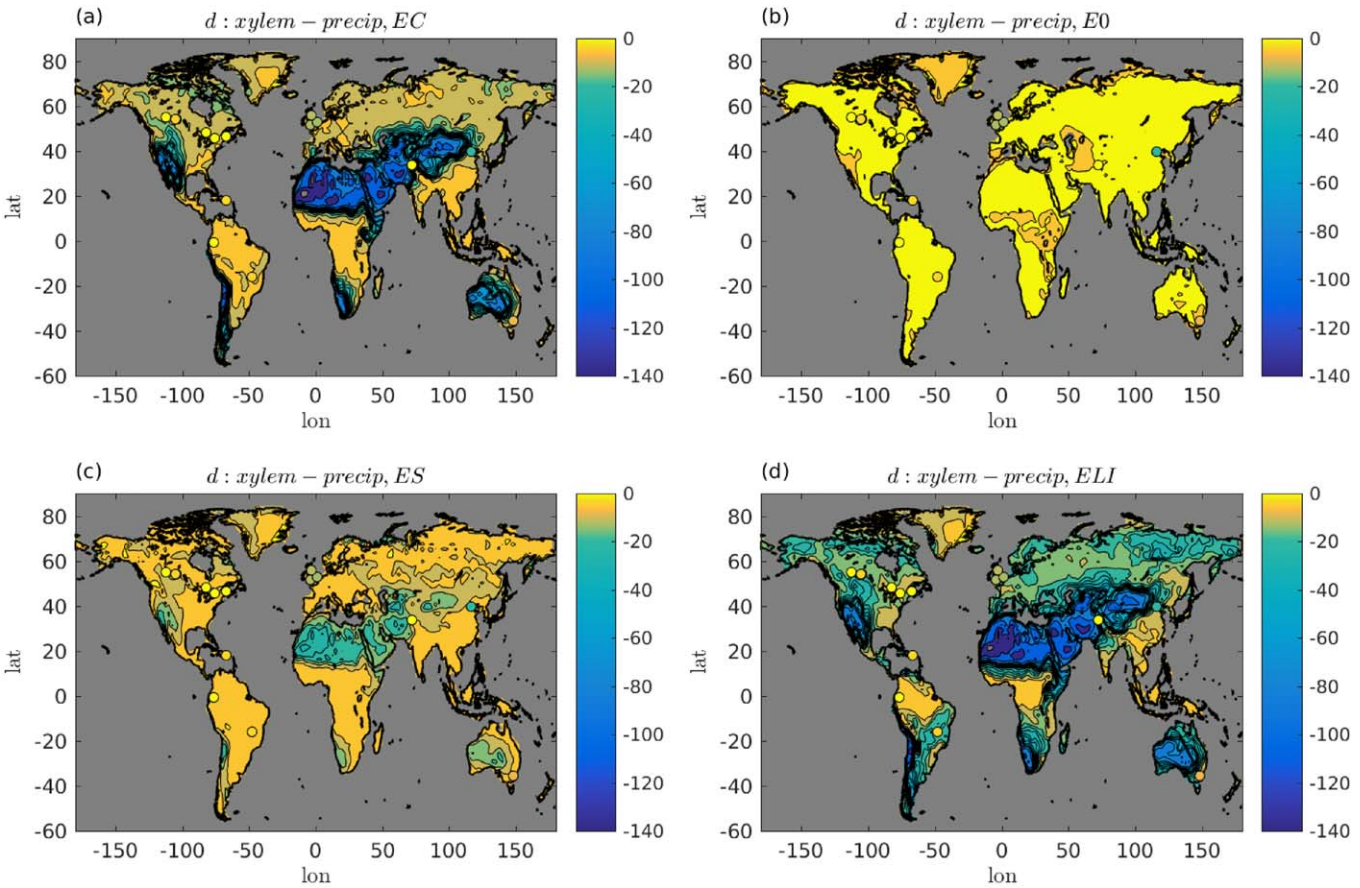

Figure 13. Comparison between iCESM-modeled and MIBA-observed xylem water deuterium excess for the sensitivity experiments: (a) EC, (b) E0, (c) ES, and (d) ELI.

that their land surface scheme alone was unable to rectify discrepancy between their modeled isotope ratios in precipitation and GNIP data. This, too, is consistent with the present work and provides confidence in both studies' conclusions regarding the land surface isotopic processes. Together, these findings suggest the need for coupled global climate model simulations to constrain the coupled climate isotopic signal, as well as an in-depth evaluation of existing theory that describes kinetic effects at ecosystem scales to constrain the individual contributions of the land and atmospheric components of the climate system. *Braud et al.* [2009] evaluated in a controlled experimental setup, the isotope ratios of evaporative fluxes from bare soils, and resulting isotope ratios on soil water and water vapor. *Rothfuss et al.* [2012] constrained estimates of isotopic kinetic effects from a calibration framework approach, demonstrating that a time-varying formulation (e.g., (MJ79)) is most appropriate. Other such controlled experiments and model experimental frameworks would be suitable for such experiments. These types of studies hold promise to assess uncertainties in existing kinetic models and where these models may best be improved.

Improvements stemming from coupled climate system simulations will include accounting for fractionating processes over lakes and wetlands [*Gibson and Edwards*, 2002], which have been neglected in the present study. This simplification likely leads to a slightly depleted bias in surface water and enriched bias in evaporation and precipitation isotope ratios. These signals are confounded by other biases introduced by coupling with an atmospheric model, the sensitivity of which is examined separately [*Nusbaumer et al.*, 2017], and is an area for continued study. For example, there is considerable difficulty in modeling high-elevation, high-precipitation regions such as the Himalayas (Figure 7a).

The site-level experiments at BAO (semiarid grassland, Erie, Colorado, USA) emphasize the need for tuning or calibrating the precise strength of parameters that control exchange fluxes and other kinetic fractionation factors in site-specific or region-specific applications. Further study using similar data sets from sites in other ecosystems is necessary to determine if these results hold in general. In spite of these inherent practical modeling

choices that must be made with care, it has been shown that (1) iCESM is capable of reliably reproducing isotopic signals in moisture data, and (2) it is critical to account for isotopic physics at the land surface (evidenced by the poor performance of the "null hypothesis" experiment E0, e.g., Figures 10 and 11).

The BAO simulations demonstrated that the hydrological connectivity in CLM4 is not strong enough, and as a result does not allow infiltration of surface water deeply enough into the soil column. This is consistent with other recent studies which have found that representation of the connectivity of the surface and deep soil moisture is a key feature for accurate soil moisture and flux modeling [*Good et al*., 2015; *Hu et al*., 2014; *Aleinov and Schmidt*, 2006]. By assimilating soil moisture data from the BAO site into the model simulation, the modeled soil water isotope ratios were brought into slightly better agreement with observed δ^{18}O ratios (mean RMSE reduced by 7%) and even better agreement with observed deuterium excess (mean RMSE reduced by 14%), even though no isotopic data were assimilated. This experiment demonstrated that a small portion of the error in iCLM4 estimates of soil water isotopic ratios stems from errors in the bulk soil hydrological scheme (compare Figures 4d and 5d). It should be noted that the biases in modeled fluxes and soil temperature were degraded as a result of the soil moisture assimilation. Thus, certain applications will require that either ensemble filtering data assimilation methods (e.g., ensemble Kalman filter) or statistical calibration schemes [e.g., *Higdon et al*., 2004] be used, so that the model and observations may be synthesized, accounting for the uncertainty inherent in each. The fact that assimilating soil moisture data does not lead to large improvements in the soil water isotopic simulation presented here points to the need to examine other potential sources of error in the isotopic model (e.g., lateral subsurface moisture transport and vapor diffusion). This use of water isotopic data to point to areas for model improvement—even in light of what might be viewed as a null result—makes progress on the need outlined by *Haese et al*. [2013] for soil moisture isotopic data capable of constraining model results, and a model capable of representing these vertically resolved data well. A single, simple field site has been used here; model comparisons with soil water isotopic data from a variety of ecosystems and climate regimes are still needed. For example, *Risi et al*. [2016] performed more detailed site-level investigations for a set of MIBA sites, similar to the site-level comparisons for BAO reviewed here. The limitations of the coarse model-data comparison presented here using the MIBA results indicates that these more detailed site-level experiments such as the BAO experiment here and the site-level MIBA experiments of *Risi et al*. [2016] offer the most promising use of the MIBA database.

These findings regarding the native CLM4 soil hydrology are largely attributed to the manner in which modeled evaporation is removed from the soil. This is an advance which was made possible only through incorporation of the present tracer scheme within CLM4. In CLM4, soil evaporation is removed from the top soil layer only, whereas recent studies have demonstrated that hydrological connectivity extends to roughly 30 cm deep into the soil column [*Wang et al*., 2010; *Good et al*., 2015]. The assumed surface soil evaporative front in CLM4 leads to the low d in the surface soil layers, and difficulty modeling the soil moisture d (Figures 4d and 5d). Improvement in the CLM4 hydrology to better account for rapid water movement in upper soil layers (such as that associated with subsurface vapor transport in arid and semiarid environments) will likely result from setting the isotope ratio of evaporation source water equal to a mass-weighted average of several of the upper layers of soil moisture. The depth to which this averaging is done should depend on the ecosystem in question, and can be determined from the evaporation front from isotopic profiles, as has been done previously [*Mathieu and Bariac*, 1996; *Wang et al*., 2010]. To account for deeper and broader evaporative fronts, the isotopic kinetic fractionation factor from *Mathieu and Bariac* [1996] would then be most appropriate for soil evaporation, and yield further improvement in the representation of land surface isotopic processes, as has been implemented in, for example, the model of *Haese et al*. [2013]. A thorough evaluation of the numerous possible formulations of the isotopic kinetic fractionation factor is beyond the scope of the present work, which sought to provide (and provide confidence in) a modeling tool to enable a wider communal effort on this frontier. Including model parameterizations for soil vapor diffusion will also yield a more realistic simulation of moisture transport through soils [*Tang et al*., 2013].

Persistent errors in the modeled bulk soil hydrology lead to errors in the isotopic simulation of soil water, which propagates into errors in modeled fluxes and other water pools. Thus, there are two main components of uncertainty leading to biases in modeled isotope ratios: uncertainty in bulk water hydrology and uncertainty in the isotopic parameterizations implemented in iCESM. An opportunity to evaluate the nonlinear dependence of soil water transport on the mean soil water state, and reduce the associated

uncertainties, exists through assimilation of newly available global soil moisture remote sensing data products. Satellite-based soil moisture data products such as the European Space Agency's Soil Moisture and Ocean Salinity (SMOS) [*Kerr et al*., 2010] and the National Aeronautics and Space Administration's Soil Moisture Active Passive (SMAP) [*Entekhabi et al*., 2010] offer viable options for assimilation data. Undoubtedly, the need to integrate newly and widely available data products with state-of-the-art physical process models, such as the one presented here, will only grow as computational power and availability of data increase.

Acknowledgments
This research is supported by the NSF Paleo Perspectives and Climate Change program (AGS-1203928 and AGS-1049104) and Climate and Large-scale Dynamics (AGS-0955841) as part of the CAREER program. We would like to acknowledge high-performance computing support from Yellowstone (ark:/85065/d7wd3xhc) provided by NCAR's Computational and Information Systems Laboratory, sponsored by the National Science Foundation. We thank Aleya Kaushik (University of Colorado) for assistance interpreting the meteorological, soil moisture, vegetation, and water isotopic data from BAO. We thank Debbie Hemming (Hadley Centre) for assistance verifying site information for the MIBA network. The analysis codes and data files are available from http://climate.ceoas.oregonstate.edu/archive/iCLM4/ as well as from the corresponding author. The iCLM4 model codes are available through the National Center for Atmospheric Research software development repository.

References

Aemisegger, F., J. Spiegel, S. Pfahl, H. Sodemann, W. Eugster, and H. Wernli (2015), Isotope meteorology of cold front passages: A case study combining observations and modeling, *Geophys. Res. Lett.*, *42*, 5652–5660, doi:10.1002/2015GL063988.

Aleinov, I., and G. Schmidt (2006), Water isotopes in the GISS ModelE land surface scheme, *Global Planet. Change*, *51*(1), 108–120.

Braud, I., P. Biron, T. Bariac, P. Richard, L. Canale, J. Gaudet, and M. Vauclin (2009), Isotopic composition of bare soil evaporated water vapor, Part I: RUBIC IV experimental setup and results, *J. Hydrol.*, *369*(1), 1–16.

Buenning, N., D. Noone, J. Randerson, W. J. Riley, and C. Still (2014), The response of the $^{18}O/^{16}O$ composition of atmospheric CO_2 to changes in environmental conditions, *J. Geophys. Res. Biogeosci.*, *119*(1), 55–79.

Cernusak, L. A., G. D. Farquhar, and J. S. Pate (2005), Environmental and physiological controls over oxygen and carbon isotope composition of Tasmanian blue gum, *Eucalyptus globulus*, *Tree Physiol.*, *25*(2), 129–146.

Craig, H., and L. I. Gordon (1965), Deuterium and oxygen 18 variations in the ocean and the marine atmosphere, in *Stable Isotopes in Oceanographic Studies and Paleotemperatures*, edited by E. Tongiorgi, pp. 9–130, V. Lishi e F., Pisa, Italy.

Crank, J., and P. Nicolson (1947), A practical method for numerical evaluation of solutions of partial differential equations of the heat-conduction type, *Proc. Cambridge Philos. Soc.*, *43*, 50–67, doi:10.1017/S0305004100023197.

Dongmann, G., H. Nürnberg, H. Förstel, and K. Wagener (1974), On the enrichment of h218o in the leaves of transpiring plants, *Radiat. Environ. Biophys.*, *11*(1), 41–52.

Entekhabi, D., et al. (2010), The Soil Moisture Active Passive (SMAP) mission, *Proc. IEEE*, *98*(5), 704–716.

Farquhar, G., and J. Lloyd (1993), Carbon and oxygen isotope effects in the exchange of carbon dioxide between terrestrial plants and the atmosphere, in *Stable Isotopes and Plant Carbon-Water Relations*, vol. 40, pp. 47–70, edited by J. R. Ehleringer, A. E. Hall, and G. D. Farquhar, Academic, San Diego, Calif.

Ferretti, D., E. Pendall, J. Morgan, J. Nelson, D. Lecain, and A. Mosier (2003), Partitioning evapotranspiration fluxes from a Colorado grassland using stable isotopes: Seasonal variations and ecosystem implications of elevated atmospheric CO_2, *Plant Soil*, *254*(2), 291–303.

Flanagan, L. B., J. P. Comstock, and J. R. Ehleringer (1991), Comparison of modeled and observed environmental influences on the stable oxygen and hydrogen isotope composition of leaf water in phaseolus vulgaris l, *Plant Physiol.*, *96*(2), 588–596.

Gibson, J., and T. Edwards (2002), Regional water balance trends and evaporation-transpiration partitioning from a stable isotope survey of lakes in northern Canada, *Global Biogeochem. Cycles*, *16*(2), 1026, doi:10.1029/2001GB001839.

Good, S. P., K. Soderberg, L. Wang, and K. K. Caylor (2012), Uncertainties in the assessment of the isotopic composition of surface fluxes: A direct comparison of techniques using laser-based water vapor isotope analyzers, *J. Geophys. Res. Atmos.*, *117*, D15301, doi:10.1029/2011JD017168.

Good, S. P., D. Noone, and G. Bowen (2015), Hydrologic connectivity constrains partitioning of global terrestrial water fluxes, *Science*, *349*(6244), 175–177.

Griffis, T. J. (2013), Tracing the flow of carbon dioxide and water vapor between the biosphere and atmosphere: A review of optical isotope techniques and their application, *Agric. For. Meteorol.*, *174*, 85–109.

Haese, B., M. Werner, and G. Lohmann (2013), Stable water isotopes in the coupled atmosphere-land surface model ECHAM5-JSBACH, *Geosci. Model Dev.*, *6*, 1463–1480.

Higdon, D., M. Kennedy, J. C. Cavendish, J. A. Cafeo, and R. D. Ryne (2004), Combining field data and computer simulations for calibration and prediction, *SIAM J. Sci. Comput.*, *26*(2), 448–466.

Horita, J., and D. J. Wesolowski (1994), Liquid-vapor fractionation of oxygen and hydrogen isotopes of water from the freezing to the critical temperature, *Geochim. Cosmochim. Acta*, *58*(16), 3425–3437.

Hu, Z., X. Wen, X. Sun, L. Li, G. Yu, X. Lee, and S. Li (2014), Partitioning of evapotranspiration through oxygen isotopic measurements of water pools and fluxes in a temperate grassland, *J. Geophys. Res. Biogeosci.*, *119*, 358–372, doi:10.1002/2013JG002367.

Hurrell, J. W., et al. (2013), The Community Earth System Model: A framework for collaborative research, *Bull. Am. Meteorol. Soc.*, *94*(9), 1339–1360.

International Atomic Energy Agency (IAEA) (1994a), International Atomic Energy Agency (IAEA), Environmental Isotope Data No. 1-10: World Survey of Isotope Concentration in Precipitation, Vienna, Austria.

International Atomic Energy Agency (IAEA) (1994b), Moisture Isotopes in the Biosphere and Atmosphere, The MIBA Database, Vienna, Austria.

International Atomic Energy Agency (IAEA) (2012), Monitoring Isotopes in Rivers: Creation of the Global Network of Isotopes in Rivers, (GNIR), *IAEA-TECDOC-1673*, Vienna, Austria.

Jasechko, S., Z. D. Sharp, J. J. Gibson, S. J. Birks, Y. Yi, and P. J. Fawcett (2013), Terrestrial water fluxes dominated by transpiration, *Nature*, *496*(7445), 347–350.

Kalman, R. E. (1960), A new approach to linear filtering and prediction problems, *J. Basic Eng.*, *82*(1), 35–45.

Keeling, C. D. (1958), The concentration and isotopic abundances of atmospheric carbon dioxide in rural areas, *Geochim. Cosmochim. Acta*, *13*(4), 322–334.

Kerr, Y. H., et al. (2010), The SMOS mission: New tool for monitoring key elements of the global water cycle, *Proc. IEEE*, *98*(5), 666–687.

Kurita, N., K. Ichiyanagi, J. Matsumoto, M. D. Yamanaka, and T. Ohata (2009), The relationship between the isotopic content of precipitation and the precipitation amount in tropical regions, *J. Geochem. Explor.*, *102*(3), 113–122.

Lee, X., T. J. Griffis, J. M. Baker, K. A. Billmark, K. Kim, and L. R. Welp (2009), Canopy-scale kinetic fractionation of atmospheric carbon dioxide and water vapor isotopes, *Global Biogeochem. Cycles*, *23*, GB1002, doi:10.1029/2008GB003331.

Mathieu, R., and T. Bariac (1996), A numerical model for the simulation of stable isotope profiles in drying soils, *J. Geophys. Res.*, *101*(D7), 12,685–12,696.

Merlivat, L. (1978), Molecular diffusivities of $H_2^{16}O$, HDO, and $H_2^{18}O$ in gases, *J. Chem. Phys.*, *69*, 2864–2871.

Merlivat, L., and J. Jouzel (1979), Global climatic interpretation of the deuterium-oxygen 18 relationship for precipitation, *J. Geophys. Res. Oceans*, *84*(C8), 5029–5033.
Moerman, J. W., K. M. Cobb, J. F. Adkins, H. Sodemann, B. Clark, and A. A. Tuen (2013), Diurnal to interannual rainfall δ^{18}O variations in northern Borneo driven by regional hydrology, *Earth Planet. Sci. Lett.*, *369*, 108–119.
Noone, D., and C. Sturm (2010), Comprehensive dynamical models of global and regional water isotope distributions, in *Isoscapes*, edited by J. B. West, pp. 195–219, Springer, Amsterdam.
Nusbaumer, J., T. E. Wong, C. Bardeen, and D. Noone (2017), Evaluating hydrological processes in the Community Atmosphere Model Version 5 (CAM5) using stable isotope ratios of water, *J. Adv. Model. Earth Syst.*, doi:10.1002/2016MS000839.
Oleson, K., et al. (2010), Technical description of version 4.0 of the Community Land Model (CLM), *Tech. Rep.*, *NCAR Tech. Note NCAR/TN-4781STR*, Natl. Cent. for Atmos. Res., Boulder, Colo.
Riley, W., C. Still, M. Torn, and J. Berry (2002), A mechanistic model of $H_2^{18}O$ and $C^{18}OO$ fluxes between ecosystems and the atmosphere: Model description and sensitivity analyses, *Global Biogeochem. Cycles*, *16*(4), 1095.
Risi, C., et al. (2012), Process-evaluation of tropospheric humidity simulated by general circulation models using water vapor isotopologues: 1. Comparison between models and observations, *J. Geophys. Res. Atmos.*, *117*, D05304, doi:10.1029/2011JD016623.
Risi, C., et al. (2016), The water isotopic version of the land-surface model ORCHIDEE: Implementation, evaluation, sensitivity to hydrological parameters, *Hydrol. Current Res.*, *7*, 258, doi:10.4172/2157-7587.1000258.
Roden, J. S., G. Lin, and J. R. Ehleringer (2000), A mechanistic model for interpretation of hydrogen and oxygen isotope ratios in tree-ring cellulose, *Geochim. Cosmochim. Acta*, *64*(1), 21–35.
Rodgers, C. D. (2000), *Inverse Methods for Atmospheric Sounding: Theory and Practice*, vol. *2*, World Sci., Singapore.
Rothfuss, Y., P. Biron, I. Braud, L. Canale, J.-L. Durand, J.-P. Gaudet, P. Richard, M. Vauclin, and T. Bariac (2010), Partitioning evapotranspiration fluxes into soil evaporation and plant transpiration using water stable isotopes under controlled conditions, *Hydrol. Processes*, *24*(22), 3177–3194.
Rothfuss, Y., I. Braud, N. Le Moine, P. Biron, J.-L. Durand, M. Vauclin, and T. Bariac (2012), Factors controlling the isotopic partitioning between soil evaporation and plant transpiration: Assessment using a multi-objective calibration of SiSPAT-Isotope under controlled conditions, *J. Hydrol.*, *442*, 75–88.
Sakaguchi, K., and X. Zeng (2009), Effects of soil wetness, plant litter, and under-canopy atmospheric stability on ground evaporation in the Community Land Model (CLM3.5), *J. Geophys. Res. Atmos.*, *114*, D01107, doi:10.1029/2008JD010834.
Sutanto, S., B. Van den Hurk, P. Dirmeyer, S. Seneviratne, T. Rockmann, K. Trenberth, E. Blyth, J. Wenninger, and G. Hoffmann (2014), HESS opinions: A perspective on isotope versus non-isotope approaches to determine the contribution of transpiration to total evaporation, *Hydrol. Earth Syst. Sci.*, *18*(8), 2815–2827.
Tang, J., W. Riley, C. Koven, and Z. Subin (2013), CLM4-BeTR, a generic biogeochemical transport and reaction module for CLM4: Model development, evaluation, and application, *Geosci. Model Dev.*, *6*(1), 127–140.
Twining, J., D. Stone, C. Tadros, A. Henderson-Sellers, and A. Williams (2006), Moisture Isotopes in the Biosphere and Atmosphere (MIBA) in Australia: A priori estimates and preliminary observations of stable water isotopes in soil, plant and vapour for the Tumbarumba Field Campaign, *Global Planet. Change*, *51*(1), 59–72.
Vitvar, T., P. K. Aggarwal, and A. L. Herczeg (2007), Global network is launched to monitor isotopes in rivers, *Eos Trans. AGU*, *88*(33), 325–326.
Wang, L., K. K. Caylor, J. C. Villegas, G. A. Barron-Gafford, D. D. Breshears, and T. E. Huxman (2010), Partitioning evapotranspiration across gradients of woody plant cover: Assessment of a stable isotope technique, *Geophys. Res. Lett.*, *37*, L09401, doi:10.1029/2010GL043228.
Wang, X.-F., and D. Yakir (2000), Using stable isotopes of water in evapotranspiration studies, *Hydrol. Processes*, *14*(8), 1407–1421.
Wassenaar, L. I., T. B. Coplen, and P. K. Aggarwal (2014), Approaches for achieving long-term accuracy and precision of δ^{18}O and δ^{2}H for waters analyzed using laser absorption spectrometers, *Environ. Sci. Technol.*, *48*(2), 1123–1131.
Wei, Z., K. Yoshimura, A. Okazaki, W. Kim, Z. Liu, and M. Yokoi (2015), Partitioning of evapotranspiration using high-frequency water vapor isotopic measurement over a rice paddy field, *Water Resour. Res.*, *51*, 3716–3729, doi:10.1002/2014WR016737.
Williams, D., et al. (2004), Evapotranspiration components determined by stable isotope, sap flow and eddy covariance techniques, *Agric. For. Meteorol.*, *125*(3), 241–258.
Xu, Z., H. Yang, F. Liu, S. An, J. Cui, Z. Wang, and S. Liu (2008), Partitioning evapotranspiration flux components in a subalpine shrubland based on stable isotopic measurements, *Bot. Stud.*, *49*(4), 351–361.
Yepez, E. A., D. G. Williams, R. L. Scott, and G. Lin (2003), Partitioning overstory and understory evapotranspiration in a semiarid savanna woodland from the isotopic composition of water vapor, *Agric. For. Meteorol.*, *119*(1), 53–68.
Yochum, S. E. (2015), Colorado Front Range Flood of 2013: Peak flows and flood frequencies, in *Proceedings of the 3rd Joint Federal Interagency Conference on Sedimentation and Hydrologic Modeling*, pp. 19–23, Reno, Nev.